Spiral order from orientationally correlated random bonds in classical XY models

Andrea Scaramucci,[1,*] Hiroshi Shinaoka,[2,3,4,†] Maxim V. Mostovoy,[5] Markus Müller,[6,7] and Christopher Mudry[6]

[1] *Laboratory for Scientific Development and Novel Materials, Paul Scherrer Institut, 5235, Villigen PSI, Switzerland*
[2] *Institute for Theoretical Physics, ETH Zürich, CH-8093 Zürich, Switzerland*
[3] *Department of Physics, University of Fribourg, 1700 Fribourg, Switzerland*
[4] *Department of Physics, Saitama University, 338-8570 Saitama, Japan*
[5] *Zernike Institute for Advanced Materials, University of Groningen, Nijenborgh 4, 9747 AG, Groningen, The Netherlands*
[6] *Condensed Matter Theory Group, Paul Scherrer Institute, CH-5232 Villigen PSI, Switzerland*
[7] *The Abdus Salam International Centre for Theoretical Physics, 34151, Trieste, Italy*

We discuss the stability of ferromagnetic long-range order in three-dimensional classical XY ferromagnets upon substitution of a small subset of equally oriented bonds by impurity bonds, on which the ferromagnetic exchange $J_\perp > 0$ is replaced by a strong antiferromagnetic coupling $J_{\rm imp} < 0$. In the impurity-free limit, the effective low-energy Hamiltonian is that of spin waves. In the presence of a single impurity bond, once the absolute value of the frustrating coupling $J_{\rm imp} < 0$ exceeds a threshold $J_{\rm c} > 0$, the ground state becomes two-fold degenerate, corresponding to either clockwise or anticlockwise canting of the spins in the vicinity of the impurity bond. In the presence of a finite but small concentration of impurity bonds, the effective low-energy Hamiltonian is that of Ising variables encoding the sense of rotation of the local canting around the impurities. Those degrees of freedom interact pairwise through a dipolar interaction mediated by spin waves. A ferromagnetic Ising ground state indicates the instability of the XY ferromagnet towards a spiral state with a wave vector proportional to the concentration of impurity bonds. To analyze under which circumstances such a ground state arises, we study first regular arrays of impurities forming a superlattice. For a subclass of those, we can rigorously establish the existence of spiral order. For another class of superlattices, the Ising variables order ferromagnetically in planes perpendicular to the orientation of impurity bonds, but antiferromagnetically parallel to it, which results in a fan-like XY ground state. Second, we consider the case when the equally oriented impurity bonds are randomly distributed on the three-dimensional host lattice according to a Poisson process. We show the phenomenon of spiral order by disorder with an ordering wave vector proportional to the dilute impurity concentration. The analytical predictions based on the effective dipolar Ising Hamiltonian are confirmed by Monte Carlo simulations of a slightly more general model of classical Heisenberg spins with easy-plane anisotropy. The latter is relevant for magnetic materials such as $YBaCuFeO_5$.

I. INTRODUCTION

Insulating magnets supporting magnetic long-range spiral order are of technological interest as they can display "magnetically" induced ferroelectricity[1–4]. In prototypical spin-spiral multiferroics, e.g., $RMnO_3$ (R=Tb^{3+}, Dy^{3+}, etc.)[5,6], a magnetic spiral phase can be stabilized by the competition between nearest-neighbor and further-neighbor magnetic exchange interactions with opposite signs[7,8]. However, the resulting frustration only induces spiral states if further-neighbor couplings are sufficiently strong as compared to nearest-neighbor couplings. The latter are typically much bigger in magnitude, except under special circumstances that lead to their suppression. In such exceptional cases, the characteristic exchange scale is set by the further-neighbor interactions and is thus very weak, entailing a low spiral ordering temperature.

In order to engineer magnetic insulators with magnetic spiral order establishing at high temperatures, it is of fundamental interest to investigate alternative mechanisms. An interesting route was suggested by the study of Ivanov et *al.*[9] who considered a Heisenberg antiferromagnet on a square lattice, in which every other horizontal nearest-neighbor bond in a staggered pattern was replaced by a ferromagnetic coupling. Sufficiently strongly frustrating bonds were shown to induce a magnetic spiral order. From the experimental side, there are interesting hints that an alternative mechanism might be tied to the presence of disorder. Indeed, certain insulating compounds containing some degree of chemical disorder were reported to stabilize magnetic spiral order[10–13] at high temperatures. For example, the transition temperatures to the magnetic spiral phase were found to range from 180 K to 310 K[12–16] in $YBaCuFeO_5$, whereby some characteristics of the spiral depend on the degree of disorder. This empiric observation suggests the possibility that, for some materials, a magnetic spiral order might be induced by some "impurity bonds" formed by nearest-neighbor magnetic ions whose exchange coupling frustrates the order that would establish in their absence. Recent Monte Carlo simulations have confirmed this conjecture in a model describing $YBaCuFeO_5$ with disorder in the spatial location of the magnetic Cu and Fe ions[17]. The latter was assumed to result in a small concentration of locally frustrating bonds along the c direction, which indeed was shown to induce magnetic spiral order in an experimentally relevant window of parameters.

In this paper, we describe and study the general mechanism that renders the ferromagnetic long-range order of classical XY spins unstable towards spiral order, if a finite fraction of the ferromagnetic interactions is replaced by sufficiently strong antiferromagnetic exchange couplings.

The general physical mechanism at work is the following. We consider a geometrically unfrustrated lattice Λ in $d > 2$ dimensions, hosting isotropic spins with a continuous symmetry. The symmetry is broken spontaneously at low temperatures, which implies the existence of Goldstone modes. Dilute but strong impurity bonds embedded in this lattice can induce local cantings which behave as "dipole type" defects with an Ising degree of freedom associated to them. The Goldstone modes mediate an interaction between the defects, decaying as r^{-d} for large separation. Correlations in the distribution of such impurity bonds (e.g., alignment along one direction) may ensure a sufficiently non-frustrated pairwise interaction between these defects so as to favor long range order in the orientation of the local cantings. This Ising-like order implies a continuous twist of the ferromagnetic order parameter density, and thus a magnetic spiral.

For simplicity, we consider a cubic host lattice Λ embedded in three-dimensional Euclidean space with the Cartesian coordinates x, y, and z. We impose a tetragonal symmetry by choosing the ferromagnetic nearest-neighbor exchange to be $J_{\parallel} > 0$ for couplings in the x-y plane and $J_{\perp} > 0$ for bonds oriented along the z-axis. We further consider a set of impurity bonds, which form a dilute subset of the nearest-neighbor bonds that are directed along the z-direction of the cubic host lattice Λ. In each impurity bond, the ferromagnetic $J_{\perp} > 0$ is replaced by the antiferromagnetic exchange coupling $J_{\rm imp} < 0$.

A single impurity bond does not destroy the ferromagnetic long-range order of the ground state. However, it does result in a canting of the classical XY spins in the vicinity of the impurity bond, provided that the local frustration is sufficiently strong, i.e., $|J_{\rm imp}| \geq J_{\rm c}$ for some threshold value $J_{\rm c} > 0$. Under these conditions the ground state is two-fold degenerate, exhibiting either a clockwise or counter-clockwise sense of the local canting. At low concentration we can thus associate a corresponding low-energy Ising degree of freedom to every impurity bond. Apart from these discrete degrees of freedom, the background ferromagnet hosts low-energy spin wave excitations. They mediate an effective interaction between the Ising degrees of freedom, which results in an effective classical Ising model with effective two-body interactions of dipolar type. Their algebraic decay at large distance is a direct consequence of the gaplessness of the spin waves. A similar effective interaction results in any system which spontaneously breaks a continuous symmetry, and thus hosts gapless Goldstone modes mediating algebraic interactions between impurity degrees of freedom.

A ferromagnetic configuration of the Ising degrees of freedom corresponds to a spiral configuration of the original XY degrees of freedom, as the local magnetization twists in the same sense across every impurity bond. The wave vector of the resulting magnetic spiral is proportional to the magnetization density of the Ising degrees of freedom, and thus, to the density of impurity bonds. We will show that such a spiral state often turns out to be the ground state of the XY system. This happens under certain conditions on the impurity bond distribution. They leave a rather wide range of parameters in which spiral order dominates. We analyze the role of impurity distributions in the specific case where the impurity bonds form a Bravais superlattice with a unit cell that is large compared to that of the cubic host lattice Λ. For certain classes of superlattices we are able to rigorously establish the presence of spiral order.

Although the analysis in this paper assumes ferromagnetic interactions for the host lattice Λ, we note that our results can be readily extended to any unfrustrated XY magnet. For example, if the lattice is bipartite and $J_{\rm imp}$ has sign opposite to $J_{\perp}$, the system can be mapped to the above described ferromagnet as follows. For every spin, a reference frame is chosen such that the unfrustrated ground state of the impurity-free system corresponds to a ferromagnetic configuration. Therefore, the low energy effective theory presented below can be extended to this larger class of magnetic insulators.

We emphasize that for the establishment of ferromagnetic order it is central that the impurity bonds are not randomly oriented. Otherwise, the pair-wise interactions between the associated Ising degrees of freedom would be strongly random in sign, which would most likely lead to spin glass order, as observed in models of dilute, randomly oriented Ising dipoles[18,19]. Since an Ising glass state generally carries no net magnetization, it would not induce a spiral state of the original XY spins. Also, in the limit of a high density of randomly oriented impurity spins, one expects long-range spin-glass order (observed directly at the level of the XY spins), since the model becomes that of a random-bond XY gauge glass, as studied by Villain[20–22].

The remainder of this paper is structured as follows. In Sec. II, we define the spin lattice model. Section III begins with the case of a single impurity bond. We then consider a small concentration of impurity bonds and derive a mapping to an effective Ising model for low energies. Section IV describes how to find the ground state of the effective Ising model when the impurity bonds realize a superlattice. The effective Ising model is solved by analytical and numerical means. Its solution is then compared to Monte Carlo simulations of a model with the same network of exchange interactions, but in which the classical XY spins are replaced by classical Heisenberg spins with an additional easy-plane anisotropy. The latter allows for close contact with experimentally realized magnets, such as $YBaCuFeO_5$, which are believed to embody the physical ingredients and mechanisms discussed above. We expect that spiral order stemming from strong impurity bonds realizing dilute Bravais superlattices is

robust to small displacements of the impurity bonds from the perfect superlattice.

II. LATTICE HAMILTONIAN FOR CLASSICAL XY SPINS

A. Definition of the XY-model

We consider a magnet of classical spins, described by two-dimensional unit vectors $\widehat{\boldsymbol{S}}_{\boldsymbol{r}}$ with $\widehat{\boldsymbol{S}}_{\boldsymbol{r}}^2 = 1$. They are located at the sites $\boldsymbol{r} = x\,\boldsymbol{x} + y\,\boldsymbol{y} + z\,\boldsymbol{z}$ $(x, y, z \in \mathbb{Z})$ of a cubic lattice Λ made of $|\Lambda|$ sites spanned by the orthonormal unit vectors $\boldsymbol{x}$, $\boldsymbol{y}$, and $\boldsymbol{z}$ of $\mathbb{R}^3$.

We consider a classical Hamiltonian

$$H_{\mathcal{L}} \coloneqq H_0 + H_{\text{imp}}. \tag{2.1a}$$

containing only nearest-neigbor interactions between spins.

The exchange energy in Eq. (2.1a)

$$H_0 \coloneqq -\frac{1}{2} \sum_{\boldsymbol{r},\boldsymbol{r}' \in \Lambda} J^{(0)}_{\boldsymbol{r},\boldsymbol{r}'}\, \widehat{\boldsymbol{S}}_{\boldsymbol{r}} \cdot \widehat{\boldsymbol{S}}_{\boldsymbol{r}'} \tag{2.1b}$$

shares the translation symmetries of the cubic lattice, for it depends only on the nearest-neighbor ferromagnetic Heisenberg exchange couplings

$$J^{(0)}_{\boldsymbol{r},\boldsymbol{r}'} \coloneqq J_{\parallel} \sum_{\boldsymbol{\alpha}=\pm\boldsymbol{x},\pm\boldsymbol{y}} \delta_{\boldsymbol{r},\boldsymbol{r}'+\boldsymbol{\alpha}} + J_{\perp} \sum_{\boldsymbol{\alpha}=\pm\boldsymbol{z}} \delta_{\boldsymbol{r},\boldsymbol{r}'+\boldsymbol{\alpha}} = J^{(0)}_{\boldsymbol{r}',\boldsymbol{r}}. \tag{2.1c}$$

The in-plane ($J_{\parallel}$) and out-of-plane ($J_{\perp}$) couplings are ferromagnetic but can be different, $0 < J_{\parallel} \neq J_{\perp}$, in which case the cubic point-group symmetry is reduced to the tetragonal one.

The contribution from the disorder in Eq. (2.1a)

$$H_{\text{imp}} \coloneqq (|J_{\text{imp}}| + J_{\perp}) \sum_{\tilde{\boldsymbol{r}} \in \mathcal{L}} \widehat{\boldsymbol{S}}_{\tilde{\boldsymbol{r}}} \cdot \widehat{\boldsymbol{S}}_{\tilde{\boldsymbol{r}}+\boldsymbol{z}} \tag{2.1d}$$

describes the presence of antiferromagnetic impurity bonds. We label them by their end point with the smallest z-coordinate. These end points form a subset $\mathcal{L}$ of the cubic host lattice points Λ. This term breaks the cubic translation symmetry. On all impurity bonds the ferromagnetic $J_{\perp} > 0$ is replaced by the antiferromagnetic coupling $J_{\text{imp}} < 0$, inducing local frustration.

Hamiltonian (2.1a) is invariant under any rotation of all spins by the same orthogonal 2×2 matrix, i.e., $H_{\mathcal{L}}$ has a global $O(2)$ symmetry.

B. Impurity-free case

Here we consider an impurity-free system, i.e., an empty set $\mathcal{L}$,

$$H_{\mathcal{L}} = H_0. \tag{2.2}$$

The ground state is ferromagnetic with all spins parallel. We choose the polar parametrization

$$\widehat{\boldsymbol{S}}_{\boldsymbol{r}} =: \cos\theta_{\boldsymbol{r}}\, \widehat{\boldsymbol{x}} + \sin\theta_{\boldsymbol{r}}\, \widehat{\boldsymbol{y}} \tag{2.3}$$

with the orthonormal basis $\widehat{\boldsymbol{x}}$ and $\widehat{\boldsymbol{y}}$ of $\mathbb{R}^2$. In this polar representation,

$$H_0 = -\frac{1}{2} \sum_{\boldsymbol{r},\boldsymbol{r}' \in \Lambda} J^{(0)}_{\boldsymbol{r},\boldsymbol{r}'}\, \cos\left(\theta_{\boldsymbol{r}} - \theta_{\boldsymbol{r}'}\right) \tag{2.4}$$

has a ferromagnetic ground state defined by

$$\theta^{\text{Ferro}}_{\boldsymbol{r}} \equiv \text{const.} \tag{2.5}$$

for all lattice sites $\boldsymbol{r}$. In this polar representation, the invariance of $H_{\mathcal{L}}$ under any global $O(2)$ symmetry becomes the invariance under the symmetry transformation

$$\theta_{\boldsymbol{r}} \to \epsilon\, \theta_{\boldsymbol{r}} + \Theta, \tag{2.6}$$

where $\epsilon = \pm 1$ and $\Theta \in [0, 2\pi[$ are arbitrary numbers independent of $\boldsymbol{r}$. The parameter $\Theta \in [0, 2\pi[$ parametrizes a proper rotation in the connected Lie group $SO(2)$. The choice $\epsilon = -1$ corresponds to an improper rotation, an orthogonal matrix in $O(2)$ with negative determinant.

At low temperatures, $T \ll J_{\perp}, J_{\parallel}$, we can use the spin-wave approximation, which assumes that the deviations from the ferromagnetic ground state (2.5) are small. In that case, the Hamiltonian (2.4) can be expanded to quadratic order in the angle differences,

$$\begin{aligned} H_0 &\approx E_{\text{FM}} + \frac{1}{4} \sum_{\boldsymbol{r},\boldsymbol{r}' \in \Lambda} J^{(0)}_{\boldsymbol{r},\boldsymbol{r}'}\, \left(\theta_{\boldsymbol{r}} - \theta_{\boldsymbol{r}'}\right)^2 \\ &= E_{\text{FM}} + \frac{1}{2} \sum_{\boldsymbol{r},\boldsymbol{r}' \in \Lambda} D^{(0)}_{\boldsymbol{r},\boldsymbol{r}'}\, \theta_{\boldsymbol{r}}\, \theta_{\boldsymbol{r}'}, \end{aligned} \tag{2.7a}$$

where

$$E_{\text{FM}} \equiv -\frac{1}{2} \sum_{\boldsymbol{r},\boldsymbol{r}' \in \Lambda} J^{(0)}_{\boldsymbol{r},\boldsymbol{r}'} \tag{2.7b}$$

is the energy of the ferromagnetic ground state, and

$$\begin{aligned} D^{(0)}_{\boldsymbol{r},\boldsymbol{r}'} &\coloneqq \left(\sum_{\boldsymbol{r}'' \in \Lambda} J^{(0)}_{\boldsymbol{r},\boldsymbol{r}''} \right) \delta_{\boldsymbol{r},\boldsymbol{r}'} - J^{(0)}_{\boldsymbol{r},\boldsymbol{r}'} \\ &= \left(4J_{\parallel} + 2J_{\perp}\right) \delta_{\boldsymbol{r},\boldsymbol{r}'} - J^{(0)}_{\boldsymbol{r},\boldsymbol{r}'} \\ &= D^{(0)}_{\boldsymbol{r}',\boldsymbol{r}} = D^{(0)}_{\boldsymbol{r},\boldsymbol{r}'} \equiv D^{(0)}_{\boldsymbol{r}'-\boldsymbol{r}} \end{aligned} \tag{2.7c}$$

is the symmetric spin-wave kernel. It only depends on the difference $\boldsymbol{r}' - \boldsymbol{r}$, which we henceforth use as the only subscript. Observe that it obeys

$$\sum_{\boldsymbol{r}' \in \Lambda} D^{(0)}_{\boldsymbol{r}'} = 0. \tag{2.8}$$

This is a consequence of spin rotational symmetry, which implies that any global orthogonal transformation (2.6)

leaves the bilinear form (2.7a) invariant. Moreover, we have the Fourier transform

$$D^{(0)}_{\boldsymbol{k}} \coloneqq \frac{1}{|\Lambda|}\sum_{\boldsymbol{r},\boldsymbol{r}'\in\Lambda} e^{-\mathrm{i}\boldsymbol{k}\cdot(\boldsymbol{r}-\boldsymbol{r}')} D^{(0)}_{\boldsymbol{r},\boldsymbol{r}'} = 2J_{\parallel}\left(2-\cos k_x-\cos k_y\right)+2J_{\perp}\left(1-\cos k_z\right) \tag{2.9}$$

for any $\boldsymbol{k}$ belonging to the Brillouin zone of the host cubic lattice Λ. We shall denote this Brillouin zone by BZ.

III. MAPPING TO AN EFFECTIVE ISING HAMILTONIAN

A. Isolated impurity bond

Let us consider the case where the set $\mathcal{L}$ in Eq. (2.1d) consists of the single bond $\langle\tilde{\boldsymbol{r}},\tilde{\boldsymbol{r}}+\boldsymbol{z}\rangle$. Far away from this bond, the spin-wave approximation (2.7) is expected to remain valid, whereas it is not assumed to hold close to the site $\tilde{\boldsymbol{r}}$. Correspondingly, we make the approximation

$$H_{\mathcal{L}} \approx E_{\mathrm{FM}} + \frac{1}{2}\sum_{\boldsymbol{r},\boldsymbol{r}'\in\Lambda} D^{(0)}_{\boldsymbol{r}-\boldsymbol{r}'}\,\theta_{\boldsymbol{r}}\,\theta_{\boldsymbol{r}'} + \left(|J_{\mathrm{imp}}|+J_{\perp}\right)\cos\left(\theta_{\tilde{\boldsymbol{r}}}-\theta_{\tilde{\boldsymbol{r}}+\boldsymbol{z}}\right). \tag{3.1}$$

Its validity will be verified in a more general context by comparison with numerical results in Sec. IV B.

We seek the deviation away from the ferromagnetic ground state, which minimizes the energy (3.1) in the presence of the single impurity bond with end points $\tilde{\boldsymbol{r}}$ and $\tilde{\boldsymbol{r}}+\boldsymbol{z}$. For every lattice site $\boldsymbol{r}$ we obtain the saddle-point equation

$$\sum_{\boldsymbol{r}'\in\Lambda} D^{(0)}_{\boldsymbol{r}-\boldsymbol{r}'}\,\theta_{\boldsymbol{r}'} = \left(|J_{\mathrm{imp}}|+J_{\perp}\right)\left(\delta_{\boldsymbol{r},\tilde{\boldsymbol{r}}}-\delta_{\boldsymbol{r},\tilde{\boldsymbol{r}}+\boldsymbol{z}}\right) \times \sin\left(\theta_{\tilde{\boldsymbol{r}}}-\theta_{\tilde{\boldsymbol{r}}+\boldsymbol{z}}\right). \tag{3.2}$$

This equation is invariant under any global orthogonal transformation (2.6).

It is convenient to introduce the inverse of the spin-wave kernel $D^{(0)}_{\boldsymbol{r}}$ as the Green function $G^{(0)}_{\boldsymbol{r}'}$ satisfying

$$\sum_{\boldsymbol{r}'\in\Lambda} G^{(0)}_{\boldsymbol{r}-\boldsymbol{r}'}\,D^{(0)}_{\boldsymbol{r}'-\boldsymbol{r}''} = \delta_{\boldsymbol{r},\boldsymbol{r}''}, \quad \forall \boldsymbol{r},\boldsymbol{r}''. \tag{3.3a}$$

Due to the zero mode (2.8) this defines the Green's function only up to a constant, which we fix by requiring $\sum_{\boldsymbol{r}\in\Lambda} G^{(0)}_{\boldsymbol{r}} = 0$. As the inverse of a symmetric kernel, $G^{(0)}_{\boldsymbol{r}-\boldsymbol{r}'}$ is symmetric, too,

$$G^{(0)}_{\boldsymbol{r}-\boldsymbol{r}'} = G^{(0)}_{\boldsymbol{r}'-\boldsymbol{r}}. \tag{3.3b}$$

Inverting Eq. (3.2), we obtain

$$\theta_{\boldsymbol{r}} = \left(|J_{\mathrm{imp}}|+J_{\perp}\right)\left(G^{(0)}_{\boldsymbol{r}-\tilde{\boldsymbol{r}}}-G^{(0)}_{\boldsymbol{r}-\tilde{\boldsymbol{r}}-\boldsymbol{z}}\right)\sin(\theta_{\tilde{\boldsymbol{r}}}-\theta_{\tilde{\boldsymbol{r}}+\boldsymbol{z}}) \tag{3.3c}$$

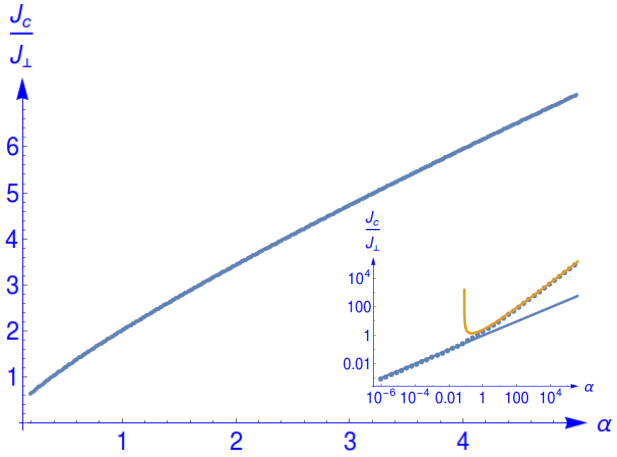

FIG. 1. (Color online) Plot of the critical impurity strength, $J_{\mathrm{c}}(\alpha)/J_{\perp}$ (blue dots), as a function of the ratio of couplings $\alpha \equiv J_{\parallel}/J_{\perp}$, whereby J_{c} is defined by Eq. (3.6a). The inset presents a logarithmic plot of $J_{\mathrm{c}}(\alpha)/J_{\perp}$ (blue dots) as a function of α. For isotropic couplings, one finds the exact value $J_{\mathrm{c}}(\alpha=1)/J_{\perp}=2$. For large anisotropies, the two predicted asymptotics $J_{\mathrm{c}}(\alpha\ll 1)/J_{\perp}\approx 0.957\sqrt{\alpha}$ (blue line) and $J_{\mathrm{c}}(\alpha\gg 1)/J_{\perp}\approx \alpha/[\ln(\alpha)/(2\pi)+C]-1$ (yellow curve) with $C\approx 0.4$ are confirmed numerically.

up to an additive constant $\Theta\in[0,2\pi[$ that remains undetermined by the saddle-point equation, since adding this zero mode to a given solution does not affect the energy. In what follows we will drop such additive constants.

Restricting Eq. (3.3c) to $\boldsymbol{r}=\tilde{\boldsymbol{r}}$ and $\boldsymbol{r}=\tilde{\boldsymbol{r}}+\boldsymbol{z}$, subtracting them, and making use of Eq. (3.3b), we obtain a closed equation obeyed by the difference of angles across the impurity bond

$$\Delta\theta_{\tilde{\boldsymbol{r}}} \equiv \theta_{\tilde{\boldsymbol{r}}}-\theta_{\tilde{\boldsymbol{r}}+\boldsymbol{z}} = \left(|J_{\mathrm{imp}}|+J_{\perp}\right)\Gamma^{(0)}_{\boldsymbol{0}}\sin\Delta\theta_{\tilde{\boldsymbol{r}}}, \tag{3.4a}$$

where

$$\Gamma^{(0)}_{\boldsymbol{0}} \coloneqq 2\left(G^{(0)}_{\boldsymbol{0}}-G^{(0)}_{\boldsymbol{z}}\right). \tag{3.4b}$$

Given a solution of this non-linear equation (3.4), the angular pattern around the single impurity bond is determined by Eq. (3.3c).

Equation (3.4) always has the trivial solution

$$\Delta\theta_{\tilde{\boldsymbol{r}}} = 0, \tag{3.5}$$

corresponding to the undistorted ferromagnetic state. However, this solution becomes unstable for $|J_{\mathrm{imp}}|$ larger than

$$J_{\mathrm{c}} \equiv \frac{1}{\Gamma^{(0)}_{\boldsymbol{0}}}-J_{\perp}. \tag{3.6a}$$

The dependence of the critical coupling on the ratio

$$\alpha \equiv \frac{J_{\parallel}}{J_{\perp}} \tag{3.6b}$$

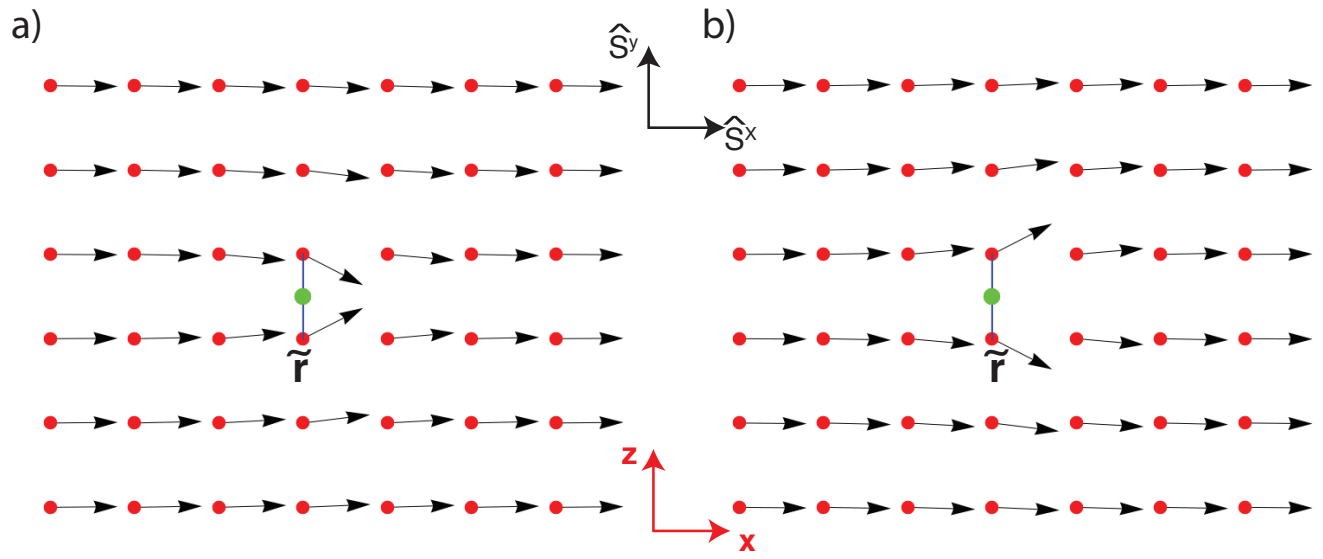

FIG. 2. (Color online) Canting induced by a single impurity bond. The two degenerate ground states correspond to the two solutions $\sigma_{\tilde{\boldsymbol{r}}} = +1$ (a) and $\sigma_{\tilde{\boldsymbol{r}}} = -1$ (b) of Eq. (3.6). Red dots indicate sites in the x-z plane (red reference frame). The black arrows represent the $\widehat{S}^x$ and $\widehat{S}^y$ components of the spins (black reference frame). The blue line indicates a frustrating antiferromagnetic bond embedded in the network of ferromagnetic couplings. The green dots indicate the inversion center with respect to which the Hamiltonian is symmetric. The operation of inversion maps the spin configurations (a) and (b) into each other.

is shown in Fig. 1.

For such strongly frustrating bonds, one finds a pair of degenerate ground states that differ in the sign of the local canting angles

$$\Delta\theta_{\tilde{\boldsymbol{r}}} = \sigma_{\tilde{\boldsymbol{r}}}\, \Delta\theta, \tag{3.6c}$$

where $\Delta\theta > 0$ is the positive solution to

$$\Delta\theta = \left(|J_{\rm imp}| + J_\perp\right)\, \Gamma_{\boldsymbol{0}}^{(0)}\, \sin\Delta\theta, \tag{3.6d}$$

while the Ising variable

$$\sigma_{\tilde{\boldsymbol{r}}} = \pm 1, \tag{3.6e}$$

captures the sense of the local canting. The closed expression

$$\Delta\theta \approx \left[6\left(1 - \frac{1}{\left(|J_{\rm imp}| + J_\perp\right)\, \Gamma_{\boldsymbol{0}}^{(0)}}\right)\right]^{1/2} \tag{3.6f}$$

is valid for small positive values of $\left(|J_{\rm imp}|/J_{\rm c}\right) - 1$. The resulting angular pattern is illustrated by the numerical solution of Eq. (3.6f) shown in Fig. 2. The canting is substantial only locally, while the ferromagnetic long-range order is restored far away from the impurity bond. At non-vanishing impurity density, the critical impurity strength is lower in general, since the interaction between impurities allows the system to lower the total energy, which renders the creation of canting patterns more favorable.

Note that the single-impurity Hamiltonian is symmetric under the inversion symmetry with respect to the bond center $\boldsymbol{R} = \tilde{\boldsymbol{r}} + \frac{\boldsymbol{z}}{2}$, i.e., $\widehat{\boldsymbol{S}}_{\boldsymbol{R}+\delta\boldsymbol{r}} \to \widehat{\boldsymbol{S}}'_{\boldsymbol{R}-\delta\boldsymbol{r}}$. The doublet of degenerate saddle points breaks this symmetry spontaneously. This pair of saddle points transform into each other under this symmetry operation.

It is instructive to derive an effective Hamiltonian describing small fluctuations about the non-trivial saddle-point (3.6). To this end, we make the Ansatz

$$\Delta\theta_{\tilde{\boldsymbol{r}}} = \Delta\theta\, \sigma_{\tilde{\boldsymbol{r}}} + \delta\theta_{\tilde{\boldsymbol{r}}} \tag{3.7}$$

and perform a Taylor expansion of $\cos\left(\theta_{\tilde{\boldsymbol{r}}} - \theta_{\tilde{\boldsymbol{r}}+\boldsymbol{z}}\right)$ in powers of $\delta\theta_{\tilde{\boldsymbol{r}}} \equiv \Delta\theta_{\tilde{\boldsymbol{r}}} - \Delta\theta\, \sigma_{\tilde{\boldsymbol{r}}}$ up to linear order, i.e.,

$$\begin{aligned}\cos\left(\theta_{\tilde{\boldsymbol{r}}} - \theta_{\tilde{\boldsymbol{r}}+\boldsymbol{z}}\right) = \cos\Delta\theta \\ - \sin(\Delta\theta)\, \left(\Delta\theta_{\tilde{\boldsymbol{r}}}\, \sigma_{\tilde{\boldsymbol{r}}} - \Delta\theta\right) \\ + \cdots .\end{aligned} \tag{3.8}$$

Insertion of

$$\theta_{\boldsymbol{r}} = \Delta\theta\, \frac{G^{(0)}_{\boldsymbol{r}-\tilde{\boldsymbol{r}}} - G^{(0)}_{\boldsymbol{r}-\tilde{\boldsymbol{r}}-\boldsymbol{z}}}{\Gamma_{\boldsymbol{0}}^{(0)}}\, \sigma_{\tilde{\boldsymbol{r}}} \tag{3.9a}$$

into the right-hand side of Eq. (3.1) with the linearization (3.8) of the impurity contribution yields an expression that is independent of $\sigma_{\tilde{\boldsymbol{r}}}$,

$$\begin{aligned}H_{\mathcal{L}}(\Delta\theta) \coloneqq E_{\rm FM} + \left(|J_{\rm imp}| + J_\perp\right)\, (\cos\Delta\theta + \Delta\theta\, \sin\Delta\theta) \\ - \frac{1}{2}\frac{(\Delta\theta)^2}{\Gamma_{\boldsymbol{0}}^{(0)}}.\end{aligned} \tag{3.9b}$$

If we introduce the constant

$$E(\Delta\theta) \coloneqq \left(|J_{\rm imp}| + J_\perp\right)\left(\cos\Delta\theta + \frac{\Delta\theta\,\sin\Delta\theta}{2}\right), \tag{3.10a}$$

we may combine Eqs. (3.9b) and (3.6d) into

$$H_{\mathcal{L}}(\Delta\theta) = E_{\rm FM} + E(\Delta\theta). \tag{3.10b}$$

We shall see that the two-fold degeneracy of the energy (3.10) that is encoded by the fact that this energy is independent of $\sigma_{\tilde{\boldsymbol{r}}}$ is lifted when we treat the case of more than one impurity bond.

In what follows, we shall need some properties of the Green function $G^{(0)}$ for the spin waves defined in Eq. (3.3a), taking full advantage of the translation symmetry of H_0. Imposing periodic boundary conditions, we have

$$G^{(0)}_{\boldsymbol{r}} = \frac{1}{|\Lambda|}\sum_{\boldsymbol{k}\in{\rm BZ}(\Lambda)\setminus\{\boldsymbol{0}\}}\frac{e^{{\rm i}\boldsymbol{k}\cdot\boldsymbol{r}}}{D^{(0)}_{\boldsymbol{k}}}, \tag{3.11}$$

where $|\Lambda|$ is the number of lattice sites in Λ, $D^{(0)}_{\boldsymbol{k}}$ was defined in Eq. (2.9), and ${\rm BZ}(\Lambda)$ denotes the Brillouin zone of the cubic host lattice Λ. Here, the term $\boldsymbol{k}=0$ is omitted in the summation over the BZ since we required that $\sum_{\boldsymbol{r}} G^{(0)}_{\boldsymbol{r}} = 0$. The self-interaction of an impurity degree of freedom is governed by

$$\Gamma^{(0)}_{\boldsymbol{0}} = 2\,(G^{(0)}_{\boldsymbol{0}} - G^{(0)}_{\boldsymbol{z}}) = \frac{1}{|\Lambda|}\sum_{\boldsymbol{k}\in{\rm BZ}(\Lambda)\setminus\{\boldsymbol{0}\}}\frac{2(1-\cos k_z)}{D^{(0)}_{\boldsymbol{k}}}, \tag{3.12}$$

while the large distance behavior of the influence of an impurity is determined by the long wavelength approximation to Eq. (3.11),

$$\begin{aligned} G^{(0)}_{\boldsymbol{r}} &\underset{|\boldsymbol{r}|\to\infty}{\sim} \int\frac{{\rm d}^3\boldsymbol{k}}{(2\pi)^3}\,\frac{e^{{\rm i}\boldsymbol{k}\cdot\boldsymbol{r}}}{J_\parallel\,\left(k_x^2+k_y^2\right)+J_\perp\,k_z^2} \\ &= \frac{1}{4\pi\sqrt{J_\parallel}}\,\frac{1}{\sqrt{J_\perp\,(x^2+y^2)+J_\parallel\,z^2}}. \end{aligned} \tag{3.13a}$$

On the right-hand side we recognize the three-dimensional Coulomb potential for the rescaled coordinates

$$\bar{x} = \sqrt{J_\perp}\,x, \qquad \bar{y} = \sqrt{J_\perp}\,y, \qquad \bar{z} = \sqrt{J_\parallel}\,z. \tag{3.13b}$$

Finally, according to Eq. (3.4), the spin canting far away from the impurity bond decays algebraically as

$$G^{(0)}_{\boldsymbol{r}-\tilde{\boldsymbol{r}}} - G^{(0)}_{\boldsymbol{r}-(\tilde{\boldsymbol{r}}+\boldsymbol{z})} \sim \partial_{\bar{z}} G^{(0)}_{\boldsymbol{r},\tilde{\boldsymbol{r}}} \sim \frac{\bar{z}}{|\bar{\boldsymbol{r}}|^3}. \tag{3.13c}$$

B. Dilute set of impurity bonds

Having established the dependence of the canting on the strength of an isolated impurity bond, we now discuss the interaction between the cantings in the presence of a non-vanishing but small concentration of impurity bonds,

$$n_{\rm imp} \coloneqq \frac{|\mathcal{L}|}{|\Lambda|} \ll 1. \tag{3.14}$$

In this limit, we again make the approximation

$$\begin{aligned} H_{\mathcal{L}} \approx E_{\rm FM} &+ \frac{1}{2}\sum_{\boldsymbol{r},\boldsymbol{r}'\in\Lambda} D^{(0)}_{\boldsymbol{r}-\boldsymbol{r}'}\,\theta_{\boldsymbol{r}}\,\theta_{\boldsymbol{r}'} \\ &+ \left(|J_{\rm imp}| + J_\perp\right)\sum_{\tilde{\boldsymbol{r}}\in\mathcal{L}}\cos\Delta\theta_{\tilde{\boldsymbol{r}}}, \end{aligned} \tag{3.15a}$$

where

$$\Delta\theta_{\tilde{\boldsymbol{r}}} \equiv \theta_{\tilde{\boldsymbol{r}}} - \theta_{\tilde{\boldsymbol{r}}+\boldsymbol{z}} \tag{3.15b}$$

denotes the difference in angles (twist angle) across an impurity bond with the end points $\tilde{\boldsymbol{r}}$ and $\tilde{\boldsymbol{r}}+\boldsymbol{z}$. Based on our discussion of a single impurity bond, we expect that the superposition of cantings induced by impurity bonds at different positions (i) mediates an effective interaction between the signs of the cantings and (ii) affects the canting magnitudes. The Hamiltonian (3.15) is invariant under any global orthogonal transformation (2.6).

Indeed, the states obtained from minimizing Eq. (3.15) follow from a straightforward generalization of the saddle-point equation (3.2) for one impurity to many impurities. Upon multiplication from the left of the many-impurities counterpart to Eq. (3.2) by the Green function $G^{(0)}$ and with the definition (3.4), one finds

$$\theta_{\boldsymbol{r}} = \left(|J_{\rm imp}| + J_\perp\right)\sum_{\tilde{\boldsymbol{r}}\in\mathcal{L}}\left(G^{(0)}_{\boldsymbol{r}-\tilde{\boldsymbol{r}}} - G^{(0)}_{\boldsymbol{r}-\tilde{\boldsymbol{r}}-\boldsymbol{z}}\right)\sin\Delta\theta_{\tilde{\boldsymbol{r}}} \tag{3.16a}$$

for any lattice site $\boldsymbol{r}$. Unlike the saddle-point equation from which it derives, Eq. (3.16a) breaks the symmetry under any global orthogonal transformation (2.6) with $\Theta \neq 0$. What remains is the Ising symmetry under the global transformation $\theta_{\boldsymbol{r}} \to -\theta_{\boldsymbol{r}}$. If we apply Eq. (3.16a) to the end points $\tilde{\boldsymbol{r}} \in \mathcal{L}$ and $\tilde{\boldsymbol{r}}+\boldsymbol{z} \in \mathcal{L}$ of an impurity bond, we

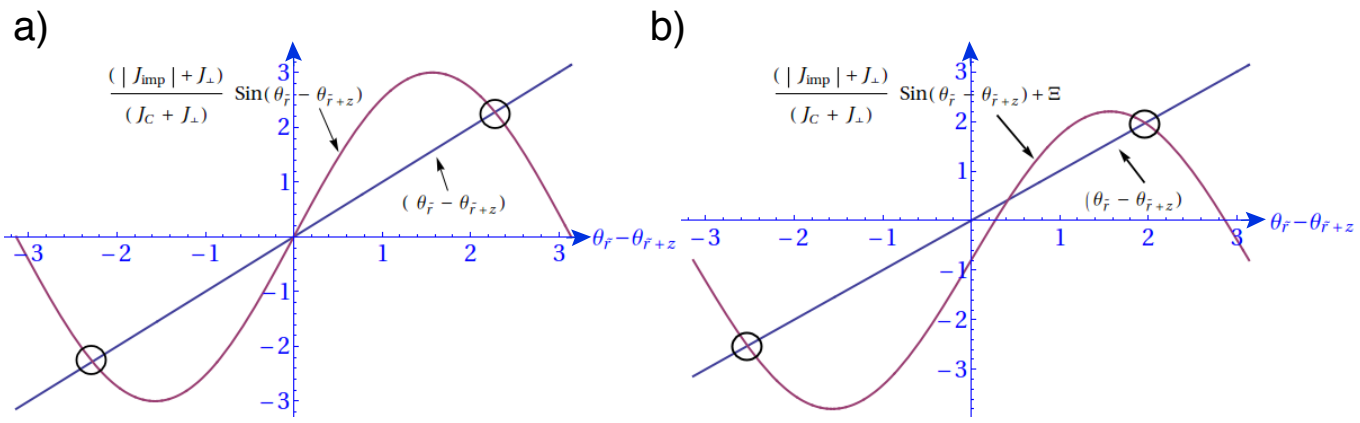

FIG. 3. (Color online) Graphical representation of the saddle-point equations (3.21) for the cases of a single antiferromagnetic impurity bond (left panel) and of a dilute density $n_{\rm imp}$ of antiferromagnetic impurity bonds (right panel). (a) The saddle-point equation (3.21) for a single antiferromagnetic impurity bond has three solutions when $J_{\rm imp} > J_{\rm c}$, one of which corresponds to the unstable ferromagnetic state and the two others (black circles) corresponding to a pair of degenerate stable solutions with opposite canting angles. (b) When condition (3.22) is met, there remain three local solutions to the saddle-point equation (3.21) that evolved smoothly from the three solutions for the single impurity limit. By continuity, the solution evolving from the ferromagnetic state is unstable, while the degeneracy of the two other solutions (black circles) is lifted.

obtain

$$\theta_{\tilde{\boldsymbol{r}}} = \left(|J_{\rm imp}| + J_\perp\right) \sum_{\tilde{\boldsymbol{r}}' \in \mathcal{L}} \left(G^{(0)}_{\tilde{\boldsymbol{r}}-\tilde{\boldsymbol{r}}'} - G^{(0)}_{\tilde{\boldsymbol{r}}-\tilde{\boldsymbol{r}}'-\boldsymbol{z}}\right) \sin\Delta\theta_{\tilde{\boldsymbol{r}}'} \tag{3.16b}$$

and

$$\theta_{\tilde{\boldsymbol{r}}+\boldsymbol{z}} = \left(|J_{\rm imp}| + J_\perp\right) \sum_{\tilde{\boldsymbol{r}}' \in \mathcal{L}} \left(G^{(0)}_{\tilde{\boldsymbol{r}}+\boldsymbol{z}-\tilde{\boldsymbol{r}}'} - G^{(0)}_{\tilde{\boldsymbol{r}}-\tilde{\boldsymbol{r}}'}\right) \sin\Delta\theta_{\tilde{\boldsymbol{r}}'}, \tag{3.16c}$$

respectively. There thus follows, for the set of twist bond angles $\Delta\theta_{\tilde{\boldsymbol{r}}} \equiv \theta_{\tilde{\boldsymbol{r}}} - \theta_{\tilde{\boldsymbol{r}}+\boldsymbol{z}}$ the closed set of $|\mathcal{L}|$ nonlinear equations

$$\Delta\theta_{\tilde{\boldsymbol{r}}} = \left(|J_{\rm imp}| + J_\perp\right) \left(\Gamma^{(0)}_{\boldsymbol{0}} \sin\Delta\theta_{\tilde{\boldsymbol{r}}} + \sum_{\tilde{\boldsymbol{r}}' \in \mathcal{L}\setminus\{\tilde{\boldsymbol{r}}\}} \Gamma^{(0)}_{\tilde{\boldsymbol{r}}-\tilde{\boldsymbol{r}}'} \sin\Delta\theta_{\tilde{\boldsymbol{r}}'} \right), \tag{3.17a}$$

where we have introduced the linear combination

$$\Gamma^{(0)}_{\tilde{\boldsymbol{r}}-\tilde{\boldsymbol{r}}'} \coloneqq 2G^{(0)}_{\tilde{\boldsymbol{r}}-\tilde{\boldsymbol{r}}'} - G^{(0)}_{\tilde{\boldsymbol{r}}-\tilde{\boldsymbol{r}}'+\boldsymbol{z}} - G^{(0)}_{\tilde{\boldsymbol{r}}-\tilde{\boldsymbol{r}}'-\boldsymbol{z}} \tag{3.17b}$$

of Green functions. As it should be, Eq. (3.17) reduces to (3.4) when $|\mathcal{L}| = 1$. Accordingly, the canting of the spins at and near an impurity bond is affected by the canting of the spins at and near all other impurity bonds through the second term on the right-hand side. Given a solution, the full angular pattern is simply determined by Eq. (3.16a).

As before the ferromagnetic state (3.5) is a solution of Eq. (3.17). However, it might not be a global minimum of the Hamiltonian. Consider a configuration of angles obeying the condition

$$\sin\left(\theta_{\tilde{\boldsymbol{r}}'} - \theta_{\tilde{\boldsymbol{r}}'+\boldsymbol{z}}\right) = \mathrm{sgn}\left(\Gamma^{(0)}_{\tilde{\boldsymbol{r}}-\tilde{\boldsymbol{r}}'}\right) \times C, \ |C| \le 1. \tag{3.18}$$

Such a configuration cannot be a solution of Eq. (3.17), as the second term on the right-hand side of Eq. (3.17a),

$$\Xi_{\tilde{\boldsymbol{r}}} \coloneqq \left(|J_{\rm imp}| + J_\perp\right) \sum_{\tilde{\boldsymbol{r}}' \in \mathcal{L}\setminus\{\tilde{\boldsymbol{r}}\}} \Gamma^{(0)}_{\tilde{\boldsymbol{r}}-\tilde{\boldsymbol{r}}'} \sin\Delta\theta_{\tilde{\boldsymbol{r}}'}, \tag{3.19}$$

would be logarithmically divergent. However, configurations of angles obeying the condition that

$$\mathrm{sgn}\Big(\sin\left(\Delta\theta_{\tilde{\boldsymbol{r}}}\right)\Big) \tag{3.20}$$

is independent of the impurity bond (labelled by $\tilde{\boldsymbol{r}}$) can be solutions of Eq. (3.17a), as $\Xi_{\tilde{\boldsymbol{r}}}$ defined by Eq. (3.19) is then a convergent alternating sum. It is convenient to rewrite Eq. (3.17), with the help of Eqs. (3.6a) and (3.19), as

$$\Delta\theta_{\tilde{\boldsymbol{r}}} = \frac{|J_{\rm imp}| + J_\perp}{J_{\rm c} + J_\perp} \sin\Delta\theta_{\tilde{\boldsymbol{r}}} + \Xi_{\tilde{\boldsymbol{r}}}. \tag{3.21}$$

From the above discussion, and using Eqs. (3.13) and (3.17b), one expects that $\Xi_{\tilde{\boldsymbol{r}}}$ scales as $n_{\rm imp}$. In that case, the condition

$$\frac{|J_{\rm imp}| + J_\perp}{J_{\rm c} + J_\perp} \gg \Xi_{\tilde{\boldsymbol{r}}} \tag{3.22}$$

can be met for sufficiently large values of $J_{\rm imp}$ and sufficiently small values of $n_{\rm imp}$. When condition (3.22) is met, we expect that solutions to Eq. (3.21) exist such that they correspond to local minima of the Hamiltonian which locally look like the solution for a single antiferromagnetic impurity bond. A graphical justification for this expectation is given in Fig. 3(b), where the left-hand-side (blue) and the right-hand-side of Eq. (3.21) (red) are sketched and compared with the solutions for a single impurity bond [Fig. 3(a)].

The fact that the limit $n_{\rm imp} \to 0$ gives a manifold of $2^{|\mathcal{L}|}$ stable and degenerate solutions to Eq. (3.21) suggests to perform a Taylor expansion of $\big(|J_{\rm imp}| + J_\perp\big) \sum_{\tilde{\boldsymbol{r}}\in\mathcal{L}} \cos\Delta\theta_{\tilde{\boldsymbol{r}}}$ in Eq. (3.15a) about any one of these degenerate saddle-points. To this end, we make the ansatz

$$\Delta\theta_{\tilde{\boldsymbol{r}}} = \sigma_{\tilde{\boldsymbol{r}}}\, \Delta\theta + \delta\theta_{\tilde{\boldsymbol{r}}} \tag{3.23}$$

for the twist angle $\Delta\theta_{\tilde{\boldsymbol{r}}} \equiv \theta_{\tilde{\boldsymbol{r}}} - \theta_{\tilde{\boldsymbol{r}}+\boldsymbol{z}}$. Here, $\Delta\theta$ is the positive solution of the single-impurity equation for the bond angle, Eq. (3.4), and $\delta\theta_{\tilde{\boldsymbol{r}}}$ is a perturbation which is small when (3.22) holds. Expanding $H_{\rm imp}$ to first order in $\delta\theta_{\tilde{\boldsymbol{r}}}$ and re-expressing it in terms of $\Delta\theta_{\tilde{\boldsymbol{r}}}$ through Eq. (3.23) yields the low-energy Hamiltonian

$$H_{\mathcal{L}} \approx E_{\rm FM} + \frac{1}{2} \sum_{\boldsymbol{r},\boldsymbol{r}'\in\Lambda} D^{(0)}_{\boldsymbol{r}-\boldsymbol{r}'}\, \theta_{\boldsymbol{r}}\, \theta_{\boldsymbol{r}'} + \big(|J_{\rm imp}| + J_\perp\big) \sum_{\tilde{\boldsymbol{r}}\in\mathcal{L}} \left[\cos\Delta\theta - \sin\Delta\theta\ (\sigma_{\tilde{\boldsymbol{r}}}\, \Delta\theta_{\tilde{\boldsymbol{r}}} - \Delta\theta)\right] \tag{3.24}$$

that is quadratic in the angles $\theta_{\boldsymbol{r}}$, $\boldsymbol{r} \in \Lambda$.

The saddle point equations for the functional (3.24) read

$$\theta_{\boldsymbol{r}} = \big(|J_{\rm imp}| + J_\perp\big)\, \sin\Delta\theta \left[\sum_{\tilde{\boldsymbol{r}}\in\mathcal{L}} \left(G^{(0)}_{\boldsymbol{r}-\tilde{\boldsymbol{r}}} - G^{(0)}_{\boldsymbol{r}-\tilde{\boldsymbol{r}}-\boldsymbol{z}}\right) \sigma_{\tilde{\boldsymbol{r}}}\right]. \tag{3.25}$$

Using them to evaluate the twist angle $\Delta\theta_{\tilde{\boldsymbol{r}}} \equiv \theta_{\tilde{\boldsymbol{r}}} - \theta_{\tilde{\boldsymbol{r}}+\boldsymbol{z}}$ across the impurity bond with the end points $\tilde{\boldsymbol{r}}$ and $\tilde{\boldsymbol{r}} + \boldsymbol{z}$, we find

$$\Delta\theta_{\tilde{\boldsymbol{r}}} = \sigma_{\tilde{\boldsymbol{r}}}\, \Delta\theta + \big(|J_{\rm imp}| + J_\perp\big)\, \sin\Delta\theta \sum_{\tilde{\boldsymbol{r}}'\in\mathcal{L}\setminus\{\tilde{\boldsymbol{r}}\}} \Gamma^{(0)}_{\tilde{\boldsymbol{r}}-\tilde{\boldsymbol{r}}'}\, \sigma_{\tilde{\boldsymbol{r}}'}, \tag{3.26}$$

which is consistent with Eq. (3.23). The energy of each extremum can be obtained by substituting the solutions (3.25) and (3.26) into Eq. (3.24), thereby delivering a functional that depends solely on the Ising degrees of freedom defined on $\mathcal{L}$,

$$H_{\mathcal{L}}(\{\sigma_{\tilde{\boldsymbol{r}}}\}) \approx E_{\rm FM} + E(\Delta\theta)\, |\mathcal{L}| - \frac{\big(|J_{\rm imp}| + J_\perp\big)^2\, \sin^2\Delta\theta}{2} \sum_{\tilde{\boldsymbol{r}}\neq\tilde{\boldsymbol{r}}'\in\mathcal{L}} \Gamma^{(0)}_{\tilde{\boldsymbol{r}}-\tilde{\boldsymbol{r}}'}\, \sigma_{\tilde{\boldsymbol{r}}}\, \sigma_{\tilde{\boldsymbol{r}}'}. \tag{3.27}$$

where the constant $E(\Delta\theta)$ was defined in Eq. (3.10b). As it should be, Eq. (3.27) reduces to Eq. (3.10) when $|\mathcal{L}| = 1$.

The original symmetry under any global orthogonal transformation (2.6) is broken down to the residual global Ising symmetry $\sigma_{\tilde{\boldsymbol{r}}} \to -\sigma_{\tilde{\boldsymbol{r}}}$ for all $\boldsymbol{r} \in \Lambda$.

The Fourier expansion

$$\begin{aligned}\Gamma^{(0)}_{\tilde{\boldsymbol{r}}-\tilde{\boldsymbol{r}}'} &\equiv \frac{1}{|\Lambda|} \sum_{\boldsymbol{k}\in{\rm BZ}(\Lambda)\setminus\{\boldsymbol{0}\}} e^{{\rm i}\boldsymbol{k}\cdot(\tilde{\boldsymbol{r}}-\tilde{\boldsymbol{r}}')}\, \Gamma^{(0)}_{\boldsymbol{k}} \\ &= \frac{1}{|\Lambda|} \sum_{\boldsymbol{k}\in{\rm BZ}(\Lambda)\setminus\{\boldsymbol{0}\}} e^{{\rm i}\boldsymbol{k}\cdot(\tilde{\boldsymbol{r}}-\tilde{\boldsymbol{r}}')}\, \frac{2(1-\cos k_z)}{D^{(0)}_{\boldsymbol{k}}}\end{aligned} \tag{3.28}$$

of the interaction between any pair of Ising variables follows from combining Eqs. (3.11) and (3.17b). At large

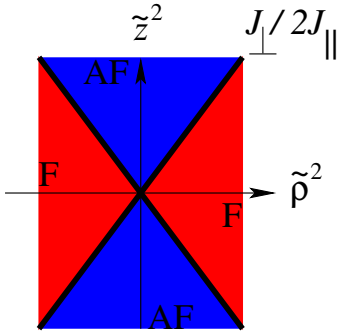

FIG. 4. (Color online) Support in the $\tilde{\rho}^2 - \tilde{z}^2$-plane (with $\tilde{\rho}^2 \equiv \tilde{x}^2 + \tilde{y}^2$) of the dipolar interaction (3.29), whereby its sign corresponds to ferromagnetic or antiferromagnetic interactions, respectively. The fraction of the $\tilde{\rho}^2 - \tilde{z}^2$-plane supporting a ferromagnetic dipolar interaction is larger than the one supporting an antiferromagnetic dipolar interaction when $J_\perp/(2J_\parallel) > 1$. In the quasi-one-dimensional limit $J_\parallel/J_\perp \to 0$, the dipolar interaction (3.29) is ferromagnetic for any $\tilde{\rho}^2 > 0$. In the quasi-two-dimensional limit $J_\perp/J_\parallel \to 0$, the dipolar interaction (3.29) is antiferromagnetic for any $\tilde{z}^2 > 0$.

distances, it can be approximated by

$$\begin{aligned}\Gamma^{(0)}_{\tilde{\boldsymbol{r}}} &\approx \int \frac{\mathrm{d}^3\boldsymbol{k}}{(2\pi)^3}\, e^{\mathrm{i}\boldsymbol{k}\cdot\tilde{\boldsymbol{r}}}\, \frac{k_z^2}{J_\parallel\left(k_x^2+k_y^2\right)+J_\perp\, k_z^2} \\ &= \frac{J_\parallel^{1/2}}{4\pi}\, \frac{J_\perp\left(\tilde{x}^2+\tilde{y}^2\right)-2J_\parallel\,\tilde{z}^2}{\left[J_\perp\,\left(\tilde{x}^2+\tilde{y}^2\right)+J_\parallel\,\tilde{z}^2\right]^{\frac{5}{2}}} \\ &= -\,\frac{\partial^2 G^{(0)}_{\tilde{\boldsymbol{r}}}}{\partial z^2}\end{aligned} \tag{3.29}$$

for any $\tilde{\boldsymbol{r}} = (\tilde{x}, \tilde{y}, \tilde{z}) \in \mathcal{L}$. This shows that, provided the density of impurity bonds is sufficiently low, the effective impurity degrees of freedom interact by a two-body interaction like that of Ising dipoles ($\sigma_{\tilde{\boldsymbol{r}}}$ oriented along the direction $\boldsymbol{z}$), albeit with the opposite sign as compared to the usual dipolar interaction. In this limit, the two-body interaction is ferromagnetic when

$$\tilde{x}^2 + \tilde{y}^2 > \frac{2J_\parallel}{J_\perp}\,\tilde{z}^2, \tag{3.30a}$$

vanishing on the conical surface

$$\tilde{x}^2 + \tilde{y}^2 = \frac{2J_\parallel}{J_\perp}\,\tilde{z}^2, \tag{3.30b}$$

and antiferromagnetic when

$$\tilde{x}^2 + \tilde{y}^2 < \frac{2J_\parallel}{J_\perp}\,\tilde{z}^2 \tag{3.30c}$$

(see Fig. 4).

C. Screw boundary conditions along the z axis

So far, we have imposed periodic boundary conditions (PBC) on the polar angles $\{\theta_{\boldsymbol{r}},\ \boldsymbol{r} \in \Lambda\}$ defined in Eq. (2.3). PBC on the angles $\{\theta_{\boldsymbol{r}},\ \boldsymbol{r} \in \Lambda\}$ preclude configurations of the $O(2)$ spins $\{\widehat{\boldsymbol{S}}_{\boldsymbol{r}},\ \boldsymbol{r} \in \Lambda\}$, that undergo a multiple of 2π rotations over their target space as $\boldsymbol{r}$ winds around the torus. In particular, PBC on the angles $\{\theta_{\boldsymbol{r}},\ \boldsymbol{r} \in \Lambda\}$ preclude spiral states. To overcome this limitation, we instead impose twisted boundary conditions on the angles $\{\theta_{\boldsymbol{r}},\ \boldsymbol{r} \in \Lambda\}$ along the $\boldsymbol{z}$-direction. This is to say that we require that

$$\theta_{\boldsymbol{r}} = \phi_{\boldsymbol{r}} + Q\,\boldsymbol{r}_z \tag{3.31}$$

holds. Here, the variable $Q \in [-\pi, \pi[$ is a global degree of freedom, while the local degrees of freedom $\phi_{\boldsymbol{r}}$ obey PBC. Q should be an integer multiple of $2\pi/L_z$, but this discrete constraint is irrelevant in the thermodynamic limit. With the change of variables (3.31), the spin-wave approximation (3.15), where the cosine of non-impurity bonds is expanded to second order, becomes

$$\begin{aligned}H_{\mathcal{L}} = E_{\mathrm{FM}} &+ \frac{1}{2}\sum_{\boldsymbol{r},\boldsymbol{r}'\in\Lambda} D^{(0)}_{\boldsymbol{r}-\boldsymbol{r}'}\,\phi_{\boldsymbol{r}}\,\phi_{\boldsymbol{r}'} + \frac{J_\perp\,Q^2}{2}\,|\Lambda| \\ &+ \left(|J_{\mathrm{imp}}| + J_\perp\right)\sum_{\tilde{\boldsymbol{r}}\in\mathcal{L}} \cos(\Delta\phi_{\tilde{\boldsymbol{r}}} - Q),\end{aligned} \tag{3.32}$$

where we recall that $|\Lambda|$ is the number of sites in the host cubic lattice Λ, and we denote by

$$\Delta\phi_{\tilde{\boldsymbol{r}}} = \phi_{\tilde{\boldsymbol{r}}} - \phi_{\tilde{\boldsymbol{r}}+z} \tag{3.33}$$

the angular twist across the impurity bond labelled by $\tilde{\boldsymbol{r}}$.

Minimization of Eq. (3.32) yields the equation

$$\Delta\phi_{\tilde{\boldsymbol{r}}} = \left(|J_{\mathrm{imp}}| + J_\perp\right)\left[2\left(G^{(0)}_{\boldsymbol{0}} - G^{(0)}_{\boldsymbol{z}}\right)\,\sin\left(\Delta\phi_{\tilde{\boldsymbol{r}}} - Q\right) + \sum_{\tilde{\boldsymbol{r}}'\in\mathcal{L}\setminus\{\tilde{\boldsymbol{r}}\}} \Gamma^{(0)}_{\tilde{\boldsymbol{r}},\tilde{\boldsymbol{r}}'}\,\sin\left(\Delta\phi_{\tilde{\boldsymbol{r}}'} - Q\right)\right] \tag{3.34}$$

for any $\boldsymbol{z}$-directed impurity bond starting at $\tilde{\boldsymbol{r}} \in \mathcal{L}$.

In the thermodynamic limit $|\Lambda| \to \infty$, and for a fixed low impurity concentration $0 < n_{\mathrm{imp}} \ll 1$, we assume,

and will verify *a posteriori*, that $|Q| \ll \Delta\theta$, where $\Delta\theta$ is the canting angle across an isolated impurity bond. Expanding $\big(|J_{\rm imp}| + J_\perp\big) \sum_{\tilde{\boldsymbol{r}}\in\mathcal{L}} \cos(\Delta\phi_{\tilde{\boldsymbol{r}}} - Q)$ again in small deviations away from $\Delta\phi_{\tilde{\boldsymbol{r}}} = \pm\Delta\theta$, i.e., up to first order in Q and in $\delta\phi_{\tilde{\mathbf{r}}} = \Delta\phi_{\tilde{\boldsymbol{r}}} - \sigma_{\tilde{\boldsymbol{r}}}\,\Delta\theta$, leads to the Hamiltonian

$$\begin{aligned} H_{\mathcal{L}} \approx E_{\rm FM} + \frac{1}{2}\sum_{\boldsymbol{r},\boldsymbol{r}'\in\Lambda} D^{(0)}_{\boldsymbol{r}-\boldsymbol{r}'}\,\phi_{\boldsymbol{r}}\,\phi_{\boldsymbol{r}'} + \big(|J_{\rm imp}| + J_\perp\big)\sum_{\tilde{\boldsymbol{r}}\in\mathcal{L}}\big[\cos\Delta\theta - \sin\Delta\theta\;(\sigma_{\tilde{\boldsymbol{r}}}\,\Delta\phi_{\tilde{\boldsymbol{r}}} - \Delta\theta)\big] \\ + \big(|J_{\rm imp}| + J_\perp\big)\,\sin\Delta\theta\, Q\sum_{\tilde{\boldsymbol{r}}\in\mathcal{L}}\sigma_{\tilde{\boldsymbol{r}}} + \frac{J_\perp\,Q^2}{2}\,|\Lambda|. \end{aligned} \tag{3.35}$$

The second term encodes the stiffness of the ferromagnetic spin waves. The third term is the local energy gain (loss) upon increasing (decreasing) the canting of the spins at an impurity bond away from the value $\sigma_{\tilde{\boldsymbol{r}}}\,\Delta\theta$. The fourth term is the energy gain (cost) for canting the spins at the impurity bonds in the same (opposite) sense as induced by the screw boundary conditions. The last term is the energy cost for applying screw boundary conditions.

Minimization of Eq. (3.35) with respect to $\phi_{\boldsymbol{r}}$ yields

$$\phi_{\boldsymbol{r}} = \big(|J_{\rm imp}| + J_\perp\big)\,\sin\Delta\theta\sum_{\tilde{\boldsymbol{r}}\in\mathcal{L}}\Big(G^{(0)}_{\boldsymbol{r},\tilde{\boldsymbol{r}}} - G^{(0)}_{\boldsymbol{r},\tilde{\boldsymbol{r}}+\boldsymbol{z}}\Big)\,\sigma_{\tilde{\boldsymbol{r}}}, \tag{3.36}$$

from which the analogue of Eq. (3.26) for the variables $\phi_{\mathbf{r}}$ follows. Minimization with respect to Q gives

$$Q = -\frac{\big(|J_{\rm imp}| + J_\perp\big)\,\sin\Delta\theta}{J_\perp}\frac{1}{|\Lambda|}\sum_{\tilde{\boldsymbol{r}}\in\mathcal{L}}\sigma_{\tilde{\boldsymbol{r}}}. \tag{3.37}$$

A net winding ($Q \neq 0$) of the spins along the $\boldsymbol{z}$ direction thus occurs for configurations with a net bias in the canting of impurity bonds. An Ising state with a net magnetization corresponds to a spiral state for the XY spins. The wave vector Q of the spiral is proportional to the magnetization density of the Ising variables.

We can now check *a posteriori* the validity of the assumption $|Q| \ll \Delta\theta$. The maximal value of $|Q|$ is given by

$$\begin{aligned} |Q|_{\rm max} &= n_{\rm imp}\,\frac{|J_{\rm imp}| + J_\perp}{J_\perp}\,\sin\Delta\theta \\ &\leq n_{\rm imp}\,\frac{|J_{\rm imp}| + J_\perp}{J_\perp}\,\Delta\theta. \end{aligned} \tag{3.38}$$

Thus, for

$$n_{\rm imp} \ll \frac{J_\perp}{|J_{\rm imp}| + J_\perp}, \tag{3.39}$$

our assumption is certainly self-consistent.

Substituting the solutions obtained from minimization with respect to the variables $\phi_{\boldsymbol{r}}$ and Q into Eq. (3.35), we obtain the effective Ising Hamiltonian governing the local cantings around the antiferromagnetic impurity bonds

$$\begin{aligned} H_{\mathcal{L}} &= E_{\rm FM} + E(\Delta\theta)\,|\mathcal{L}| \\ &\quad - \frac{1}{2}\sum_{\tilde{\boldsymbol{r}}\neq\tilde{\boldsymbol{r}}'\in\mathcal{L}} J^{(\rm I)}_{\tilde{\boldsymbol{r}}-\tilde{\boldsymbol{r}}'}\,\sigma_{\tilde{\boldsymbol{r}}}\,\sigma_{\tilde{\boldsymbol{r}}'} - \frac{\gamma\,n_{\rm imp}}{J_\perp}. \end{aligned} \tag{3.40a}$$

Here, we have introduced the constant

$$\gamma \coloneqq \frac{\big(|J_{\rm imp}| + J_\perp\big)^2\,\sin^2\Delta\theta}{2} \tag{3.40b}$$

and the Ising exchange coupling

$$J^{(\rm I)}_{\tilde{\boldsymbol{r}}-\tilde{\boldsymbol{r}}'} \coloneqq \big(|J_{\rm imp}| + J_\perp\big)^2\,\sin^2\Delta\theta\,\left(\Gamma^{(0)}_{\tilde{\boldsymbol{r}}-\tilde{\boldsymbol{r}}'} + \frac{1}{J_\perp\,|\Lambda|}\right). \tag{3.40c}$$

The original symmetry under any global orthogonal transformation (2.6) is broken down to the residual global Ising symmetry $\sigma_{\tilde{\boldsymbol{r}}} \to -\sigma_{\tilde{\boldsymbol{r}}}$ for all $\boldsymbol{r} \in \Lambda$.

Since $\Gamma^{(0)}_{\tilde{\boldsymbol{r}}-\tilde{\boldsymbol{r}}'}$ decays with $|\tilde{\boldsymbol{r}} - \tilde{\boldsymbol{r}}'|$ as $|\tilde{\boldsymbol{r}} - \tilde{\boldsymbol{r}}'|^{-3}$, the right-hand side of Eq. (3.40a) scales as $|\mathcal{L}|^2/N$. There are two additive contributions to the Ising exchange coupling $J^{(\rm I)}_{\tilde{\boldsymbol{r}}-\tilde{\boldsymbol{r}}'}$. The contribution $\Gamma^{(0)}_{\tilde{\boldsymbol{r}}-\tilde{\boldsymbol{r}}'}$ represents an (anti)-dipolar two-body interaction between the effective Ising degrees of freedom $\sigma_{\tilde{\boldsymbol{r}}}$ associated with the dilute antiferromagnetic bonds. This interaction is long ranged and frustrated owing to the indefinite sign of the kernel $\Gamma^{(0)}_{\tilde{\boldsymbol{r}}-\tilde{\boldsymbol{r}}'}$. The contribution $\frac{1}{J_\perp\,|\Lambda|}$ favors a net bias of the cantings $\sigma_{\tilde{\boldsymbol{r}}}$. Owing to the saddle-point equation (3.37), a uniform magnetization of the Ising spins $\sigma_{\tilde{\boldsymbol{r}}}$ favors a spiral state with a nonvanishing Q for the original $O(2)$ spin degrees of freedom. Hence, if the ground state of Eq. (3.40) supports a non-vanishing Q, then the magnetic frustration induced by the dilute impurity bonds turns the pristine ferromagnetic order of the impurity-free ground state into spiral order. If the ground state supports $Q = 0$, a state with a vanishing net winding of the spins is induced, such as for instance a fan-like magnetic state.

IV. SUPERLATTICES OF IMPURITY BONDS

As Eq. (3.40) involves long-range two-body interactions whose sign depends on the relative positions of the

impurity bonds, the ground state cannot be found explicitly for an arbitrary choice of $\mathcal{L}$, so that one must resort to numerical methods, or to approximate treatments.

However, if $\mathcal{L}$ realizes certain Bravais superlattices, it is possible to establish a sufficient condition for the ground state of the effective Ising Hamiltonian (3.35) to be ferromagnetic and, thus, for the ground-state spin configuration of Hamiltonian (3.24) to be a spiral.

A. Analytical considerations

We consider the case where the subset $\mathcal{L}$ of the cubic host lattice Λ forms a Bravais lattice with the basis vectors $\boldsymbol{A}$, $\boldsymbol{B}$, and $\boldsymbol{C}$ given by three independent linear combinations with integer-valued coefficients of $\boldsymbol{a} \equiv (1,0,0)^{\mathsf{T}}$, $\boldsymbol{b} \equiv (0,1,0)^{\mathsf{T}}$, and $\boldsymbol{c} \equiv (0,0,1)^{\mathsf{T}}$. The concentration of the impurity bonds is

$$n_{\mathrm{imp}} \equiv \frac{1}{|\boldsymbol{A} \cdot (\boldsymbol{B} \wedge \boldsymbol{C})|}. \tag{4.1}$$

In reciprocal space, the superlattice $\mathcal{L}$ defines a Brillouin zone $\mathrm{BZ}(\mathcal{L})$ contained $1/n_{\mathrm{imp}}$ times inside the Brillouin zone $\mathrm{BZ}(\Lambda)$ of the cubic host lattice Λ.

For the $|\mathcal{L}|$ Ising degrees of freedom $\sigma_{\tilde{\boldsymbol{r}}}$ for the impurities with $\tilde{\boldsymbol{r}} \in \mathcal{L}$, we use the Fourier representation over the Brillouin zone $\mathrm{BZ}(\mathcal{L})$,

$$\sigma_{\tilde{\boldsymbol{r}}} = \frac{1}{|\mathcal{L}|} \sum_{\boldsymbol{q} \in \mathrm{BZ}(\mathcal{L})} e^{\mathrm{i}\boldsymbol{q}\cdot\tilde{\boldsymbol{r}}}\, \sigma_{\boldsymbol{q}}. \tag{4.2}$$

For any $\boldsymbol{p} \in \mathbb{R}^3$, we shall make use of the identity

$$\frac{1}{|\mathcal{L}|} \sum_{\tilde{\boldsymbol{r}} \in \mathcal{L}} e^{\mathrm{i}\boldsymbol{p}\cdot\tilde{\boldsymbol{r}}} = \sum_{\mathsf{G} \in \mathcal{L}^\star} \delta_{\boldsymbol{p},\mathsf{G}}, \tag{4.3}$$

where $\mathcal{L}^\star$ denotes the reciprocal lattice of $\mathcal{L}$. Now, the effective Ising Hamiltonian (3.40) has the Fourier representation over the Brillouin zone $\mathrm{BZ}(\mathcal{L})$ given by

$$\begin{aligned} H_{\mathcal{L}} = {} & E_{\mathrm{FM}} + E(\Delta\theta)\,|\mathcal{L}| \\ & + \frac{\gamma}{|\mathcal{L}|} \sum_{\boldsymbol{q} \in \mathrm{BZ}(\mathcal{L})} \Upsilon_{\boldsymbol{q}}\, \sigma_{+\boldsymbol{q}}\, \sigma_{-\boldsymbol{q}}, \end{aligned} \tag{4.4a}$$

where we recall that γ was defined by Eq. (3.40b) and

$$\begin{aligned} \Upsilon_{\boldsymbol{q}} \coloneqq {} & -\sum_{\tilde{\boldsymbol{r}} \in \mathcal{L}\setminus\{\boldsymbol{0}\}} e^{-\mathrm{i}\boldsymbol{q}\cdot\tilde{\boldsymbol{r}}}\, \Gamma^{(0)}_{\tilde{\boldsymbol{r}}} - \frac{n_{\mathrm{imp}}}{J_\perp}\, \delta_{\boldsymbol{q},\boldsymbol{0}} \\ = {} & -n_{\mathrm{imp}} \sum_{\substack{\mathsf{G} \in \mathcal{L}^\star \\ \boldsymbol{q}+\mathsf{G} \in \mathrm{BZ}(\Lambda)}} \Gamma^{(0)}_{\boldsymbol{q}+\mathsf{G}} + \Gamma^{(0)}_{\boldsymbol{r}=\boldsymbol{0}} - \frac{n_{\mathrm{imp}}}{J_\perp} \delta_{\boldsymbol{q},\boldsymbol{0}}. \end{aligned} \tag{4.4b}$$

For a generic choice of the Bravais lattice $\mathcal{L}$ and of the couplings $J_\perp$, $J_\parallel$, and J_{imp}, the ground state of Hamiltonian (4.4) cannot be found in closed form. However, in the special case when the global minimum of the kernel (4.4b) over the reduced Brillouin zone $\mathrm{BZ}(\mathcal{L})$ occurs at a unique momentum $\boldsymbol{q}_{\min}$ for which the condition

$$\sigma^{\min}_{\tilde{\boldsymbol{r}}} = e^{\mathrm{i}\boldsymbol{q}_{\min}\cdot\tilde{\boldsymbol{r}}} = \pm 1 \tag{4.5}$$

holds for all $\tilde{\boldsymbol{r}} \in \mathcal{L}$, the ground state of the Ising Hamiltonian is given by Eq. (4.5). Inserting it into Eqs. (3.31), (3.36), and (3.37), and using the Fourier representation (3.11), one finds

$$\theta^{\min}_{\boldsymbol{r}} = \phi^{\min}_{\boldsymbol{r}} + Q^{\min}\, \boldsymbol{r}_z, \tag{4.6a}$$

where

$$\phi^{\min}_{\boldsymbol{r}} = n_{\mathrm{imp}} \left(|J_{\mathrm{imp}}| + J_\perp\right) \sin\Delta\theta \sum_{\left\{\boldsymbol{k} \in \mathrm{BZ}(\Lambda) \,|\, \boldsymbol{k}-\boldsymbol{q}_{\min} \in \mathcal{L}^\star \setminus \{\boldsymbol{0}\}\right\}} \frac{\left(1 - e^{-\mathrm{i}k_z}\right)\, e^{\mathrm{i}\boldsymbol{k}\cdot\boldsymbol{r}}}{2J_\parallel \left(2 - \cos k_x - \cos k_y\right) + 2J_\perp \left(1 - \cos k_z\right)}, \tag{4.6b}$$

$$Q^{\min} = -\frac{\left(|J_{\mathrm{imp}}| + J_\perp\right) \sin\Delta\theta}{J_\perp\, |\Lambda|} \sum_{\tilde{\boldsymbol{r}} \in \mathcal{L}} \sigma^{\min}_{\tilde{\boldsymbol{r}}}. \tag{4.6c}$$

Examples of $\boldsymbol{q}_{\min}$ for which Eq. (4.5) holds are

$$\boldsymbol{q}_{\min} = \boldsymbol{0} \tag{4.7a}$$

and

$$\boldsymbol{q}_{\min} \in \left\{ \pm\frac{1}{2}\, \boldsymbol{A}^\star, \pm\frac{1}{2}\, \boldsymbol{B}^\star, \pm\frac{1}{2}\, \boldsymbol{C}^\star \right\}, \tag{4.7b}$$

where $\boldsymbol{A}^\star$, $\boldsymbol{B}^\star$, and $\boldsymbol{C}^\star$ are the basis vectors of the reciprocal lattice $\mathcal{L}^\star$. In the former case, the ground state is an $O(2)$ magnetic spiral, for $Q^{\min} \neq 0$, while there is no spiral in the latter case, since $Q^{\min} = 0$.

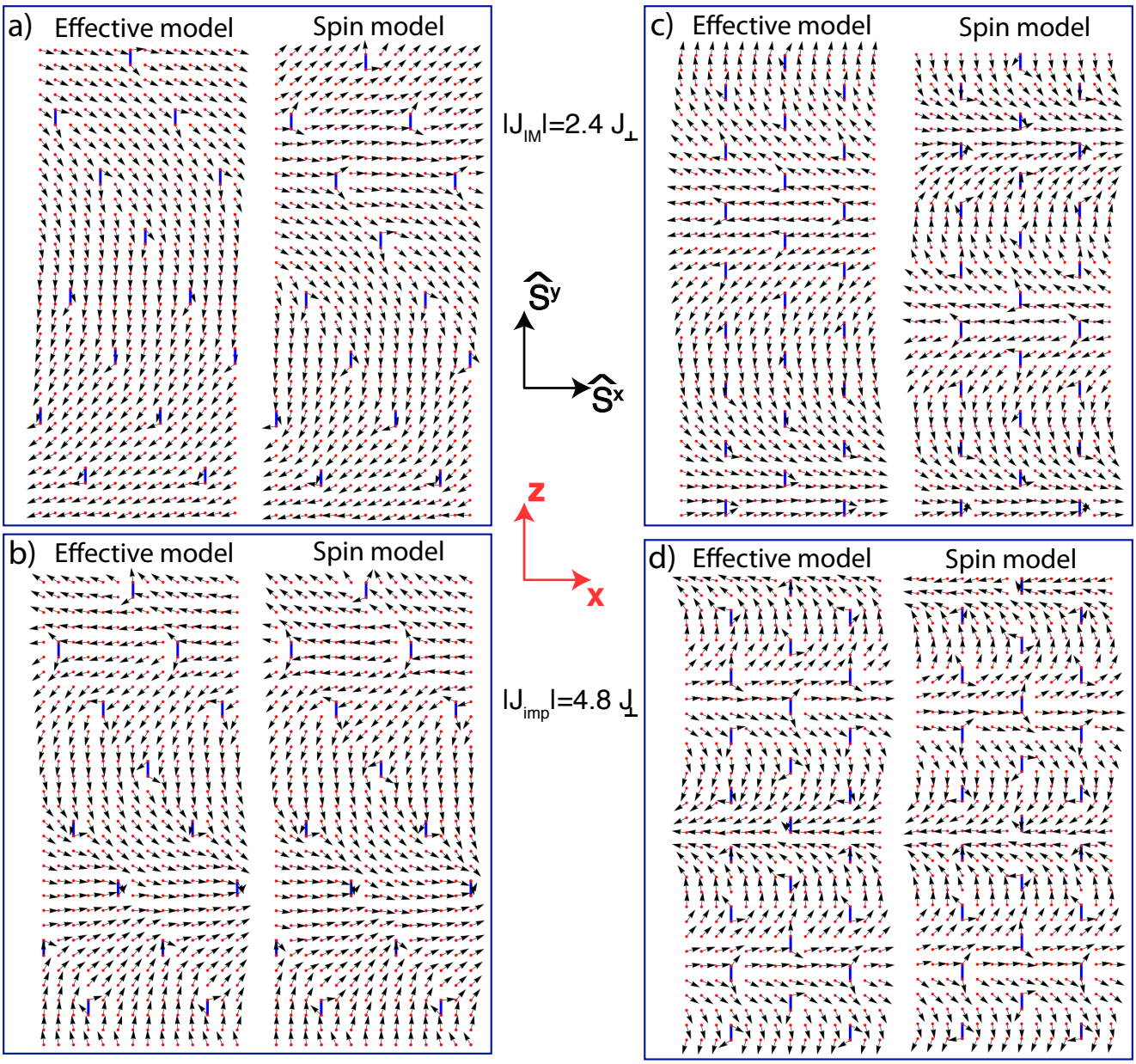

FIG. 5. (Color online) Spin configurations for the ground state in an x-z plane of the cubic host lattice Λ. Black arrows represent the $O(2)$ (XY) spins defined in Eq. (2.3) (black reference frame). Red dots represent the sites in a cross section of the cubic host lattice Λ (red reference frame). Blue lines represent the impurity bonds. Results are obtained for $J_{\parallel}/J_{\perp} = 1$. Panels (a) and (b) show the comparison between approximate analytical results (as described in the text) and MC simulations, respectively, for a superlattice with the basis $\boldsymbol{A} = (5,3,2)^{\mathsf{T}}$, $\boldsymbol{B} = (3,4,4)^{\mathsf{T}}$, and $\boldsymbol{C} = (4,5,2)^{\mathsf{T}}$. The superlattice in panels (c) and (d) has the basis $\boldsymbol{A} = (3,3,2)^{\mathsf{T}}$, $\boldsymbol{B} = (0,4,2)^{\mathsf{T}}$, and $\boldsymbol{C} = (4,0,2)^{\mathsf{T}}$. The impurity strengths are $|J_{\mathrm{imp}}/J_{\perp}| = 2.4$ for panels (a,c) and $|J_{\mathrm{imp}}/J_{\perp}| = 4.8$ for panels (b,d). While the effective model from which the approximate analytical prediction for Q follows successfully predicts a spiral state for all cases, the accuracy of the predicted value for Q improves with increasing $|J_{\mathrm{imp}}/J_{\perp}|$.

B. Comparison between analytical and numerical results for superlattices

To show that the effective Ising Hamiltonian (3.40) captures the low-energy physics of the microscopic Hamiltonian (2.1), we consider several superlattices $\mathcal{L}$ of impurity bonds and compare their microscopic ground states to the ground states of the effective Ising Hamiltonian (4.4).

Instead of directly studying the ground state of the microscopic Hamiltonian (2.1), we actually study the mi-

croscopic Hamiltonian

$$H_{\text{Heis}} \coloneqq -\frac{1}{2}\sum_{\boldsymbol{r},\boldsymbol{r}'\in\Lambda} J^{(0)}_{\boldsymbol{r},\boldsymbol{r}'}\,\boldsymbol{S}_{\boldsymbol{r}}\cdot\boldsymbol{S}_{\boldsymbol{r}'} + \big(|J_{\text{imp}}|+J_\perp\big)\sum_{\tilde{\boldsymbol{r}}\in\mathcal{L}}\boldsymbol{S}_{\tilde{\boldsymbol{r}}}\cdot\boldsymbol{S}_{\tilde{\boldsymbol{r}}+\boldsymbol{z}} + \Delta\sum_{\boldsymbol{r}}(S^z_{\boldsymbol{r}})^2, \tag{4.8}$$

which is closer to experimental realizations. Here, we have replaced the classical XY spins from Eq. (2.1) with classical Heisenberg spins $\boldsymbol{S}_{\boldsymbol{r}}$, i.e., $\boldsymbol{S}_{\boldsymbol{r}}$ is a unit vector in $\mathbb{R}^3$, A single-ion anisotropy $\Delta > 0$ penalizes an orientation along the $\boldsymbol{z}$-axis. We apply open boundary conditions along all principal directions of the cubic lattice. To approximately find the ground state, we perform parallel tempering Monte Carlo (MC) simulations. We used 140 temperatures distributed exponentially from $T \leq 4\cdot 10^{-3}$ $J_\parallel$ up to temperatures well in the paramagnetic phase. The ground state is obtained by keeping track of the minimal energy state visited during the Monte Carlo evolution for the lowest temperature. The typical value for the single-ion anisotropy $\Delta > 0$ obeys the bound ≤ 0.02 $|J_\parallel|$. When $T \ll \Delta$, the low-energy states are coplanar to a good approximation. This justifies identifying the ground state of the XY Hamiltonian (2.1) with that of the anisotropic Heisenberg Hamiltonian (4.8). The typical size of the cubic host lattice Λ used in the MC simulations is $14\times 14\times 32$ lattice spacings.

The analytical approximation is obtained from the following procedure. First, we determine if the exchange couplings allow Eq. (3.4) to have solutions $\Delta\theta \neq 0$. If so, we establish the effective Ising model of impurity degrees of freedom and seek its ground state. Finally, the local polar representation (2.3) of the $O(2)$ spins are obtained from Eq. (4.6). To determine the ground state of the Ising model, we minimize the function $\Upsilon_{\boldsymbol{q}}$ in Eq. (4.4b) with respect to $\boldsymbol{q}$. If the absolute minimum in the Brillouin zone $\text{BZ}(\mathcal{L})$ occurs at $\boldsymbol{q}=0$, we predict a spiral ground state ($Q\neq 0$). Using the value of $\Delta\theta$ obtained by solving Eq. (3.4), the local polar representation (2.3) of the $O(2)$ spins on the cubic host lattice Λ are obtained from Eq. (4.6). If instead the absolute minimum in the Brillouin zone $\text{BZ}(\mathcal{L})$ occurs at $\boldsymbol{q}_{\min} = \frac{\boldsymbol{C}^\star}{2}$, a ground state with $Q=0$ is predicted. For absolute minima occurring at $q_{\min}$ for which Eq. (4.5) does not hold for all $\tilde{\boldsymbol{r}}\in\mathcal{L}$ the ground state has more than one Fourier component and no conclusion can be drawn from our simple analysis.

Figure 5 compares the approximate ground state obtained via the effective Ising Hamiltonian (4.4a) (shown on the left) with the ground state of Hamiltonian 4.8 obtained via MC simulation (shown on the right), for two sets of impurity couplings and two superlattices. We chose parameters such that both methods yield a spiral state, with $\boldsymbol{q}_{\min}=0$ minimizing the kernel $\Upsilon_{\boldsymbol{q}}$. No coupling anisotropy ($J_\parallel/J_\perp = 1$) was assumed in all these cases. Figures 5(a) and 5(b) correspond to the same superlattice, but different impurity strengths $|J_{\text{imp}}|/J_\perp$ (equal to 2.4 and 4.8, respectively). Although a spiral magnetic ground state is correctly predicted in both cases, the canting angles at the impurity bonds and the wave vector Q of the spiral are underestimated by the effective Ising Hamiltonian, when the value of $|J_{\text{imp}}|/J_\perp = 2.4$ is small [panel (a)]. The agreement between the analytical approximation and the MC simulations improves with increasing $|J_{\text{imp}}|/J_\perp = 4.8$ [panel (b)], as expected from the considerations of Sec. III B. Indeed, the inequality (3.22) is better met for the latter value of J_{imp}, meaning that the self-interaction term in Eq. (3.17a) dominates the coupling to the other impurity bonds.

Similar results are found for other superlattices. For instance, panels (c) and (d) show results for a denser superlattice, but with the same exchange couplings as in panels (a) and (b), respectively. In all panels of Fig. 5, the deviations from the local ferromagnetic order at non-impurity bonds are small, justifying *a posteriori* the small angle approximation used to derive the effective Ising Hamiltonian (4.4).

To quantify the quality of the approximation incurred when trading the microscopic Hamiltonian (4.8) for the effective Ising Hamiltonian (4.4), we calculate for several superlattices and various ratios $|J_{\text{imp}}|/J_\perp$

$$P = \frac{1}{L_x\,L_y\,(L_z-1)}\sum_{\substack{\boldsymbol{r}\\ 1\leq r_z\leq L_z-1}} \sin\left(\phi_{\boldsymbol{r}+\boldsymbol{z}}-\phi_{\boldsymbol{r}}\right), \tag{4.9}$$

where L_x, L_y, and L_z are the linear dimensions of the lattice. This quantity is an order parameter for the magnetic spiral phase. On the right-hand side, the sine of the relative angle between $\widehat{\boldsymbol{S}}_{\boldsymbol{r}}$ and $\widehat{\boldsymbol{S}}_{\boldsymbol{r}+\boldsymbol{z}}$ is summed over all sites of the cubic host lattice Λ.

Figure 6(a) shows how $|P|$ depends on $|J_{\text{imp}}|/J_\perp$ for a few superlattices that induce a spiral state (again assuming no anisotropy, $J_\parallel/J_\perp = 1$). It can be seen that as $|J_{\text{imp}}|/J_\perp$ increases, the results for the effective Ising Hamiltonian (4.4) (dots) come closer to the results for the microscopic Hamiltonian (4.8) (squares). This is in agreement with the discussion around Eq. (3.22) and the regime of validity for the effective Ising Hamiltonian (4.4). Conversely, we note that in the regime $J_{\text{imp}} \sim J_{\text{c}}$, for which the cantings are small, the effective Ising Hamiltonian (4.4) is not quantitatively valid, since the local canting is additionally stabilized by neighboring impurities, which increases the effective value of $\Delta\theta$. In particular, we still find a finite $P\neq 0$, even when $J_{\text{imp}}/J_\perp \lesssim J_{\text{c}}$.

It is argued in Ref. 17 that the magnetic spiral order in the insulator $YBaCuFeO_5$ is driven by the physics captured by the effective Ising Hamiltonian (3.40) with $J_\parallel = 28.9$ meV, $J_{\text{imp}} = -95.8$ meV, and $J_\perp = 4.1$ meV (in Fig. 6(b) we use the average of the absolute values of the alternating couplings along the c direction presented in Ref. 17 for $J_\perp$). Figure 6(b) compares the J_{imp}

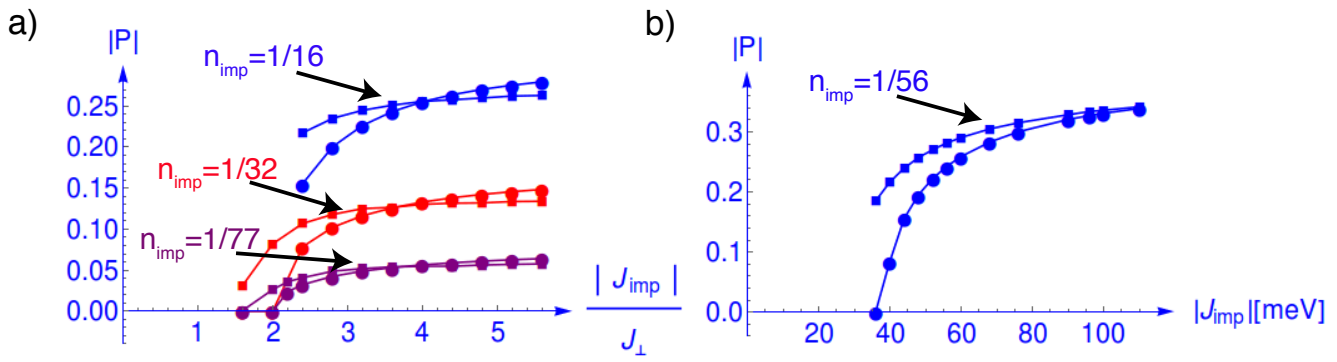

FIG. 6. (Color online) Comparison between the approximate analytical (dots) and numerical (squares) values of $|P|$ with P defined in Eq. (4.9) for XY-spins on a cubic lattice with $L_x = 14$, $L_y = 14$, and $L_z = 32$. The impurity bonds form a superlattice. Panel (a) shows the results for the isotropic case $J_\parallel/J_\perp = 1$ for three superlattices with the following basis vectors: (blue): $\boldsymbol{A} = (3,3,2)^{\mathsf{T}}$, $\boldsymbol{B} = (0,4,2)^{\mathsf{T}}$, and $\boldsymbol{C} = (4,0,2)^{\mathsf{T}}$, $n_{\rm imp} = 1/16$; (red): $\boldsymbol{A} = (5,3,2)^{\mathsf{T}}$, $\boldsymbol{B} = (3,4,4)^{\mathsf{T}}$, and $\boldsymbol{C} = (4,5,2)^{\mathsf{T}}$, $n_{\rm imp} = 1/32$; (purple): $A = (4,3,0)^{\mathsf{T}}$, $B = (0,4,3)^{\mathsf{T}}$, and $C = (5,0,2)^{\mathsf{T}}$, $n_{\rm imp} = 1/77$. Panel (b) shows the $|J_{\rm imp}|$ dependence of $|P|$. Here, we use magnetic couplings appropriate to $YBaCuFeO_5$, namely $J_\parallel = 28.9$ meV and $J_\perp = 4.1$ meV, where $J_\perp$ is taken as the average of the two couplings $J_\perp$, $J'_\perp$ in Ref. 17. This is done for a superlattice with the basis $\boldsymbol{A} = (4,3,0)^{\mathsf{T}}$, $\boldsymbol{B} = (0,4,2)^{\mathsf{T}}$, and $\boldsymbol{C} = (4,0,2)^{\mathsf{T}}$, $n_{\rm imp} = 1/56$.

dependence of P for the microscopic Hamiltonian (4.8) (squares) with that for the effective Ising Hamiltonian (4.4) (dots) when the impurity bonds realize a superlattice that stabilizes a long-range spiral order. Again, good agreement is found once the canting of a single isolated impurities is strong. The corresponding approximate and true ground states are compared in Fig. 7 for $|J_{\rm imp}| \gg J_{\rm c} \approx 39$ meV, where the approximation works very well. In Fig. 7, the superlattice is such that impurity bonds only couple every other pair of adjacent layers. In this case, spin canting mostly occurs between the layers coupled by impurity bonds.

Finally, we also consider superlattices of impurity bonds which yield a minimum of $\Upsilon_{\boldsymbol{q}}$ at $\boldsymbol{q}_{\rm min} \neq 0$. One example is shown in Fig. 8 where the value of the exchange couplings are the same as those in Fig. 7, but the superlattice favors a minimum of $\Upsilon_{\boldsymbol{q}}$ at $\boldsymbol{q}_{\rm min} = \boldsymbol{C}^\star/2$. In this case, there is no net winding of the spins, and the ground state is a fan-like state for which the magnetization of the layers alternates between even and odd planes. In other words, the magnetization rotates back and forth as the z coordinate of the planes increases. The fan state is favored because the nearest neighbors that are most strongly coupled to a given impurity degree of freedom are those located directly above and below along the z-axis. Those are antiferromagnetic in nature and thus favor cantings with an orientation that alternates between (double) layers. Instead, superlattices for which the closest neighbors belong to adjacent layers, and are thus preferentially ferromagnetically coupled, tend to stabilize spirals.

We have verified using MC simulations of the microscopic Hamiltonian (4.8) that the long-range spiral order present when the impurity bonds realize a certain Bravais superlattice is robust to weak distortions of that lattice, as expected on theoretical grounds.

V. SPIRAL ORDER IN THE DILUTE LIMIT OF RANDOM IMPURITIES

In this section we argue that in the limit of a low concentration of randomly located impurity bonds, $n_{\rm imp} \ll 1$, ferromagnetic order prevails at the level of the Ising degrees of freedom of the local cantings, implying spiral order for the original XY spin degrees of freedom.

A. Dilute tetragonal and face-centered tetragonal superlattices

Let us first discuss the case for which the impurity bonds occupy a cubic sublattice $\mathcal{L}$ of the cubic host lattice Λ. While this will turn out to support antiferromagnetic order, we will be able to use the insights brought about by this calculation for the disordered case. Moreover, it will be helpful to contrast this regular arrangement of impurities with a random distribution which sustains ferromagnetic order.

When the number of sites $|\mathcal{L}|$ in the superlattice and $|\Lambda|$ in the cubic host lattice Λ are finite and not too large, evaluation of the energy (3.40a) for all Ising spin configurations is possible by exact evaluation of the Ising kernel $J^{(\rm I)}_{\tilde{\boldsymbol{r}}-\tilde{\boldsymbol{r}}'}$ defined in Eq. (3.40c). In the thermodynamic limit, $|\Lambda| \to \infty$, with $n_{\rm imp}$ held fixed, this approach is not possible anymore. Instead, we shall restrict ourselves to a few ordered Ising configurations, which have a good chance to realize the ground state, and compare their energies.

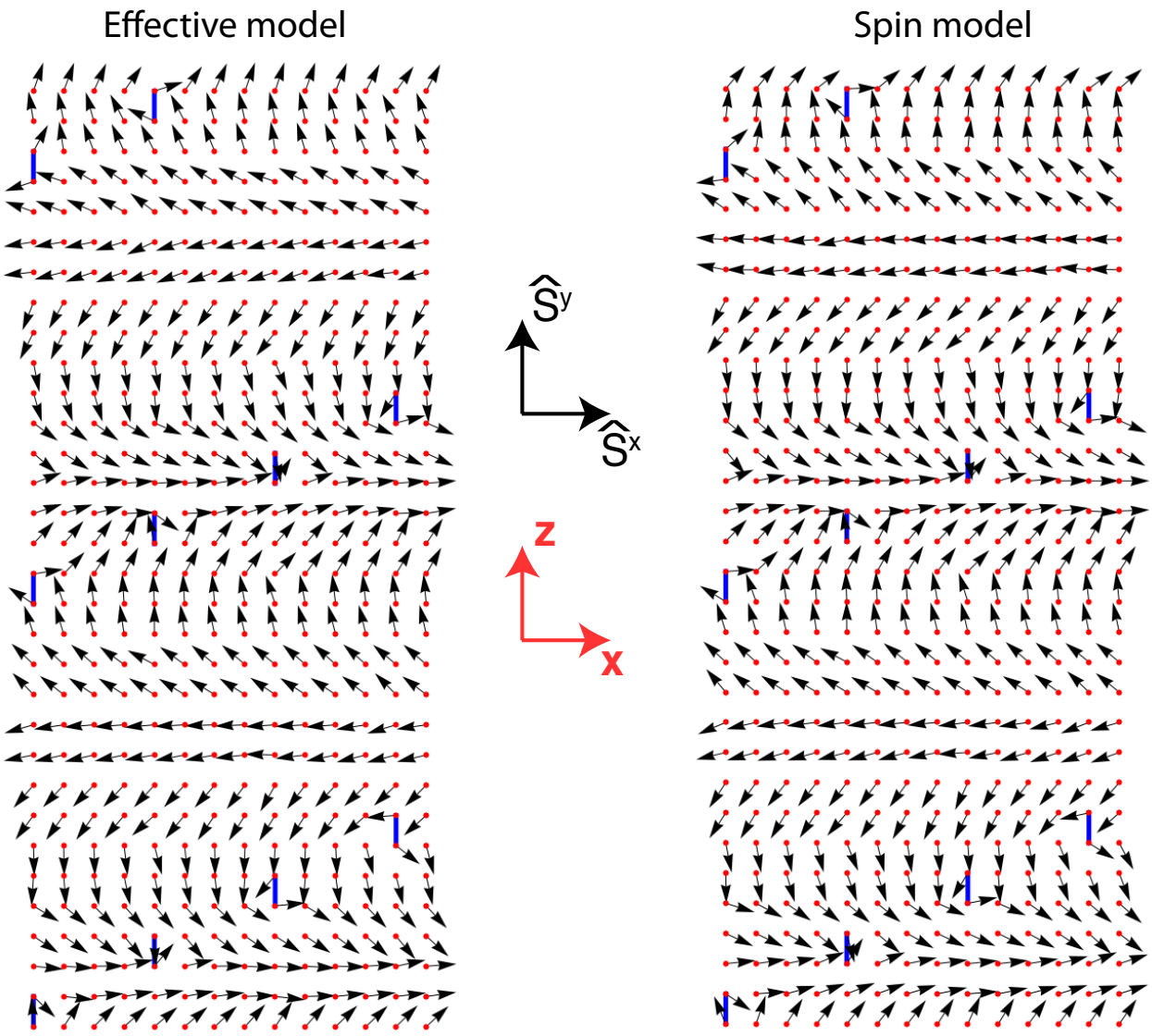

FIG. 7. (Color online) Comparison between the ground states obtained from the effective Ising Hamiltonian (4.4) (left) and the microscopic Hamiltonian (4.8) (right). The impurity bonds realize a superlattice with the basis $\boldsymbol{A} = (4,3,0)^{\mathsf{T}}$, $\boldsymbol{B} = (0,4,2)^{\mathsf{T}}$, and $\boldsymbol{C} = (4,0,2)^{\mathsf{T}}$ ($n_{\mathrm{imp}} = 1/56$). The ground state is a spiral as seen from the almost uniform winding of the spins with increasing z coordinate. The exchange couplings take the values $J_{\parallel} = 28.9$ meV, $J_{\mathrm{imp}} = -95.8$ meV, and $J_{\perp} = 4.1$ meV. These values mimick those for the compound $YBaCuFeO_5$.

The ferromagnetic Ising configuration is described by

$$\sigma^{\mathrm{F}}_{\tilde{\boldsymbol{r}}} \coloneqq 1, \qquad \frac{1}{|\Lambda|} \sum_{\tilde{\boldsymbol{r}} \in \mathcal{L}} \sigma^{\mathrm{F}}_{\tilde{\boldsymbol{r}}} = n_{\mathrm{imp}}. \tag{5.1a}$$

The most relevant competing states have ferromagnetic order in plane (as favored by the ferromagnetic interactions in the xy-plane), but antiferromagnetic order along the z-axis. We consider the family of states defined by $[\tilde{\boldsymbol{r}} = (\tilde{x}, \tilde{y}, \tilde{z})]$

$$\sigma^{\mathrm{AF}(m)}_{\tilde{\boldsymbol{r}}} \coloneqq (-1)^{\lfloor \tilde{z}/m\,\ell \rfloor}, \qquad \frac{1}{|\Lambda|} \sum_{\tilde{\boldsymbol{r}} \in \mathcal{L}} \sigma^{\mathrm{AF}(m)}_{\tilde{\boldsymbol{r}}} = 0, \tag{5.1b}$$

which describes a sequence of stacks of $m \geq 1$ layers, whose magnetization alternates. Here, $\ell \equiv n_{\mathrm{imp}}^{-1/3}$ denotes the lattice spacing of the cubic superlattice, and $\lfloor \tilde{z}/m\,\ell \rfloor$ returns the integer part of the real-valued number $\tilde{z}/m\,\ell$.

After subtraction of the constants E_{FM}, $E(\Delta\theta)\,|\mathcal{L}|$, and $-\gamma\, n_{\mathrm{imp}}/J_{\perp}$ on the right-hand side of Eq. (3.40a), the energy per impurity bond of the configurations $\mathrm{C} \in \{\mathrm{F}, \mathrm{AF}(m)\}$ is given by

$$\varepsilon^{\mathrm{C}}_{\mathcal{L}} = -\gamma \left(\sum_{\tilde{\boldsymbol{r}} \in \mathcal{L} \setminus \{\boldsymbol{0}\}} \Gamma^{(0)}_{\tilde{\boldsymbol{r}}}\, f^{\mathrm{C}}(\tilde{z}) + \frac{n_{\mathrm{imp}}}{J_{\perp}}\, \delta_{\mathrm{C,F}} \right), \tag{5.2a}$$

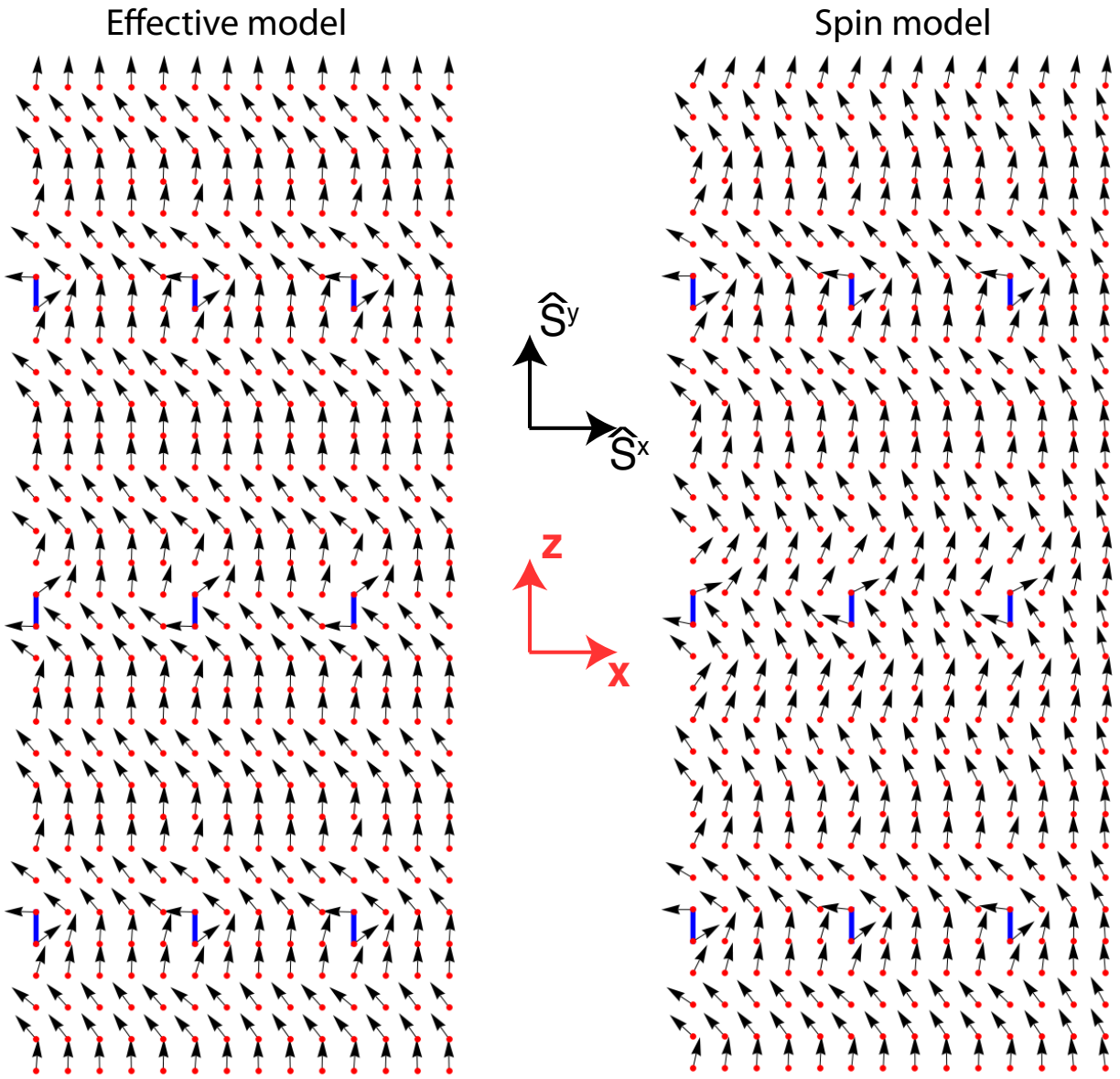

FIG. 8. (Color online) Comparison between the non-spiral ground states obtained from the effective Ising Hamiltonian (4.4) (left) and the microscopic Hamiltonian (2.1) (right). Here, the impurity bonds realize a superlattice with the basis $\boldsymbol{A} = (5, 0, 0)^{\mathsf{T}}$, $\boldsymbol{B} = (0, 5, 0)^{\mathsf{T}}$, and $\boldsymbol{C} = (0, 1, 2)^{\mathsf{T}}$ ($n_{\mathrm{imp}} = 1/50$). The exchange couplings used are the same as those used for Fig. 7. For these values the minimum of $\Upsilon_{\boldsymbol{q}}$ is at $\boldsymbol{q}_{\mathrm{min}} = \boldsymbol{C}^\star/2$ and the ground state configuration has $Q = 0$. The spins form a fan-like state instead of a spiral.

where the spin autocorrelation function

$$f^{\mathrm{C}}(\tilde{\boldsymbol{r}}) \equiv \langle \sigma_{\tilde{\boldsymbol{r}}'}\, \sigma_{\tilde{\boldsymbol{r}}'+\tilde{\boldsymbol{r}}} \rangle_{\tilde{\boldsymbol{r}}'} = f^{\mathrm{C}}(\tilde{z}) \tag{5.2b}$$

only depends on the difference in the $\tilde{z}$ coordinate, owing to Eq. (5.1). Here, $\langle \ldots \rangle_{\tilde{\boldsymbol{r}}'}$ denotes the average over the sites $\tilde{\boldsymbol{r}}'$ of the superlattice $\mathcal{L}$.

In the dilute limit $n_{\mathrm{imp}} \to 0$, the typical distance between a pair of nearest-neighbor impurities is large. Hence, the typical pair-wise interaction $\Gamma^{(0)}_{\tilde{\boldsymbol{r}}}$ tends to the dipolar form (3.29) and can be safely used to evaluate $\varepsilon^{\mathrm{AF}(m)}_{\mathcal{L}}$ up to corrections which vanish as $n_{\mathrm{imp}} \to 0$. The case of the ferromagnetic configuration is more subtle, however. Indeed a naive use of Eq. (3.29) would suggest that the first term in the right-hand side of Eq. (5.2a) vanishes, while in fact it does not. This is due to corrections to the dipolar interaction (3.29) that scale as the inverse of the volume, adding up to a finite contribution when summed with equal signs over the whole superlattice. In the case of an isotropically shaped, cubic sample with $L_x = L_y = L_z$ and isotropic interactions $J_\parallel = J_\perp \equiv J$, the computation can be done exactly, using the fact that upon averaging over all the permuta-

tions $k_x \to k_y \to k_z \to k_x$ the kernel $\Gamma^{(0)}_{\boldsymbol{k}}$ reduces to the constant $1/3$. This allows us to evaluate the lattice sum

$$\begin{aligned}\sum_{\boldsymbol{r}\in\mathcal{L}\setminus\{\boldsymbol{0}\}} \Gamma^{(0)}_{\boldsymbol{r}} &= \frac{1}{3J\,|\Lambda|} \sum_{\boldsymbol{r}\in\mathcal{L}\setminus\{\boldsymbol{0}\}} \sum_{\boldsymbol{k}\in \mathrm{BZ}(\Lambda)\setminus\{\boldsymbol{0}\}} e^{\mathrm{i}\boldsymbol{k}\cdot\boldsymbol{r}} \\ &= \frac{1}{3J\,|\Lambda|} \sum_{\boldsymbol{r}\in\mathcal{L}\setminus\{\boldsymbol{0}\}} \left(N\,\delta_{\boldsymbol{r},\boldsymbol{0}} - 1\right) \\ &= -\frac{1}{3J}\frac{|\mathcal{L}|-1}{|\Lambda|} \\ &= -\frac{n_{\mathrm{imp}}}{3J} + \mathcal{O}\left(\frac{1}{|\Lambda|}\right) \end{aligned} \tag{5.3}$$

exactly for any impurity density. This finite, negative contribution disfavors the ferromagnet. Its value varies both with the anisotropy $J_\parallel/J_\perp$ and the sample shape. Restricting ourselves to the isotropic case and inserting Eq. (5.3) into Eq. (5.2a), we obtain

$$\varepsilon^{\mathrm{F}}_{\mathcal{L}} = -\frac{2}{3}\,\frac{\gamma\, n_{\mathrm{imp}}}{J_\perp}. \tag{5.4}$$

It is useful to cast the energy (5.2a) for the ferromagnetic configuration (5.1a) of the Ising variables in a different form, namely,

$$\begin{aligned}\frac{\varepsilon^{\mathrm{F}}_{\mathcal{L}}}{\gamma} &= -\sum_{\tilde{\boldsymbol{r}}\in\mathcal{L}} \Gamma^{(0)}_{\tilde{\boldsymbol{r}}} + \Gamma^{(0)}_{\tilde{\boldsymbol{r}}=\boldsymbol{0}} - \frac{n_{\mathrm{imp}}}{J_\perp} \\ &= -\frac{1}{|\Lambda|}\sum_{\tilde{\boldsymbol{r}}\in\mathcal{L}}\sum_{\boldsymbol{k}\in\mathrm{BZ}(\Lambda)} e^{\mathrm{i}\boldsymbol{k}\cdot\tilde{\boldsymbol{r}}}\,\Gamma^{(0)}_{\boldsymbol{k}} + \Gamma^{(0)}_{\tilde{\boldsymbol{r}}=\boldsymbol{0}} - \frac{n_{\mathrm{imp}}}{J_\perp} \\ &= -\frac{|\mathcal{L}|}{|\Lambda|}\sum_{\substack{\boldsymbol{k}\in\mathrm{BZ}(\Lambda)\\ \boldsymbol{k}\in\mathcal{L}^\star}} \Gamma^{(0)}_{\boldsymbol{k}} + \Gamma^{(0)}_{\tilde{\boldsymbol{r}}=\boldsymbol{0}} - \frac{n_{\mathrm{imp}}}{J_\perp}. \end{aligned} \tag{5.5}$$

Here, the Fourier components of the interaction take the form

$$\Gamma^{(0)}_{\boldsymbol{k}} = \frac{1-\cos k_z}{J_\parallel\,\left(2-\cos k_x-\cos k_y\right) + J_\perp\,\left(1-\cos k_z\right)}, \tag{5.6}$$

and we define it to vanish at $\boldsymbol{k}=0$, where it becomes a discontinuous function of $\boldsymbol{k}\in\mathrm{BZ}(\Lambda)$ in the thermodynamic limit $|\Lambda|\to\infty$. The self-interaction

$$\Gamma^{(0)}_{\tilde{\boldsymbol{r}}=\boldsymbol{0}} \equiv \frac{1}{|\Lambda|}\sum_{\boldsymbol{k}\in\mathrm{BZ}(\Lambda)} \Gamma^{(0)}_{\boldsymbol{k}} \tag{5.7}$$

is subtracted on the right-hand side of Eq. (5.5). Similarly, one finds for the antiferromagnet AF(1) the expression

$$\begin{aligned}\frac{\varepsilon^{\mathrm{AF}(1)}_{\mathcal{L}}}{\gamma} &= -\sum_{\tilde{\boldsymbol{r}}\in\mathcal{L}} \Gamma^{(0)}_{\tilde{\boldsymbol{r}}}\,(-1)^{\lfloor \tilde{z}/\ell\rfloor} + \Gamma^{(0)}_{\tilde{\boldsymbol{r}}=\boldsymbol{0}} \\ &= -\frac{|\mathcal{L}|}{|\Lambda|}\sum_{\substack{\boldsymbol{k}\in\mathrm{BZ}(\Lambda)\\ \boldsymbol{k}+(0,0,\pi/\ell)^{\mathsf{T}}\in\mathcal{L}^\star}} \Gamma^{(0)}_{\boldsymbol{k}} + \Gamma^{(0)}_{\tilde{\boldsymbol{r}}=\boldsymbol{0}}. \end{aligned} \tag{5.8}$$

Even though the relationship between the effective Ising Hamiltonian (3.40) and the XY Hamiltonian (2.1) holds for low densities of impurity bonds, it is useful to treat the effective Ising Hamiltonian (3.40) in its own right, i.e., without requiring the impurity bonds to be dilute within the host lattice.

A maximally dense superlattice is defined by

$$\ell = 1, \qquad \mathcal{L} = \Lambda, \qquad n_{\mathrm{imp}} = \frac{|\mathcal{L}|}{|\Lambda|} = 1. \tag{5.9}$$

For a maximally dense superlattice, one finds the ferromagnetic (F) and antiferromagnetic [AF(1)] states to be degenerate,

$$\frac{\varepsilon^{\mathrm{F}}_{\mathcal{L}} - \varepsilon^{\mathrm{AF}(1)}_{\mathcal{L}}}{\gamma\, n_{\mathrm{imp}}} = \Gamma^{(0)}_{(0,0,\pi/\ell)^{\mathsf{T}}} - \Gamma^{(0)}_{\boldsymbol{k}=\boldsymbol{0}} - \frac{1}{J_\perp} = 0, \tag{5.10}$$

since

$$\Gamma^{(0)}_{(0,0,k_z)^{\mathsf{T}}} = \frac{1-\delta_{k_z,0}}{J_\perp}. \tag{5.11}$$

The identity (5.11) obeyed by the kernel (5.6) can be used together with the expression (4.4a) and the fact that only $\boldsymbol{q}$ of the form $(0,0,k_z)^{\mathsf{T}}$ enter it, to show that for a maximally dense superlattice *all* antiferromagnetic states AF(m) are degenerate with the ferromagnet. More generally, it is shown in appendix A that *any* Ising configuration where all spins of any plane at fixed z coordinate are ferromagnetically aligned, is degenerate with the ferromagnet, irrespectively of the global magnetization.

This degeneracy is lifted, however, at finite dilution, whereby the way in which the dilution is realized is crucial. For example, diluting the impurity density n_{imp} by maintaining a cubic superlattice, but increasing its integer lattice spacing ℓ disfavors the ferromagnetic state. This is illustrated in Fig. 9, where we plot the energies per impurity as a function of superlattice spacing ℓ. For small ℓ the energy difference is obtained from the representations (5.5) and (5.8). In the dilute limit, $n_{\mathrm{imp}} = \ell^{-3} \to 0$, we may also replace $1-\cos k_i$ in the kernel (5.6) by n_i^2 with $n_i \in \mathbb{Z}$ for $i = x, y, z$, i.e.,

$$\frac{\varepsilon^{\mathrm{F}}_{\mathcal{L}} - \varepsilon^{\mathrm{AF}(1)}_{\mathcal{L}}}{\gamma\, n_{\mathrm{imp}}} \to \frac{\delta(\alpha)}{J_\perp} \tag{5.12a}$$

with α defined in Eq. (3.6b) and

$$\begin{aligned}\delta(\alpha) \coloneqq -1 - \sum_{\boldsymbol{n}\in\mathbb{Z}^3\setminus\boldsymbol{0}} \Bigg[&\frac{n_z^2}{\alpha\left(n_x^2+n_y^2\right)+n_z^2} \\ &- \left(n_z \to n_z + \frac{1}{2}\right)\Bigg]. \end{aligned} \tag{5.12b}$$

The sum over n_z can be carried out explicitly and yields

$$\delta(\alpha) = \sum_{\boldsymbol{n}\in\mathbb{Z}^2\setminus\{\boldsymbol{0}\}} \frac{2\pi\sqrt{\alpha\left(n_x^2+n_y^2\right)}}{\sinh\left(2\pi\sqrt{\alpha(n_x^2+n_y^2)}\right)}, \tag{5.13}$$

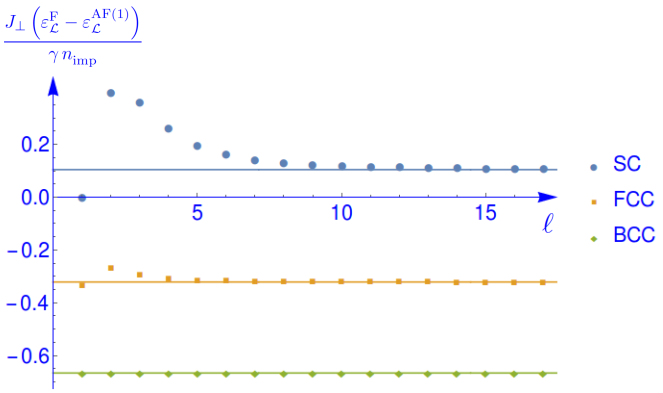

FIG. 9. (Color online) Dependence of the energy difference between the Ising ferromagnetic (F) and antiferromagnetic [AFM(1)] states on the linear size ℓ of the unit cell of the superlattice for different classes of superlattices. Blue dots represent a simple cubic (SC) superlattice with the basis vectors $(\ell,0,0)$, $(0,\ell,0)$, and $(0,0,\ell)$. Yellow squares represent a face centered cubic (FCC) superlattice with lattice vectors $(\ell,\ell,0)$, $(\ell,0,\ell)$, and $(0,\ell,\ell)$. Green diamonds represent body centered cubic (BCC) superlattices with the lattice vectors (ℓ,ℓ,ℓ), $(\ell,-\ell,\ell)$, and $(\ell,\ell,-\ell)$. The correspondingly colored horizontal solid lines represent the dilute limit $\ell\to\infty$ of these energy differences for each superlattice.

which is always positive. For the isotropic limit $\alpha=1$, one finds $\delta(1)\approx 0.1042$.

Alternatively, one can calculate the antiferromagnetic energy directly in real space using the dipolar form (3.29). This can be used to calculate the energies of other antiferromagnetic states AF(m), which all scale as

$$\frac{\varepsilon_{\mathcal{L}}^{\rm AF(m)}}{\gamma\, n_{\rm imp}}=-\frac{c_m}{J_\perp}. \tag{5.14}$$

From the above results it follows $c_1=\delta(1)+2/3$, while one finds the higher c_m's to decrease monotonically with increasing m. From this we conclude that a dilute cubic superlattice orders antiferromagnetically with layer magnetizations that alternate in sign ($m=1$).

One readily generalizes the above to tetragonal superlattices $\mathcal{L}$ with the unit vectors $(A\ell,0,0)^{\mathsf T}$, $(0,A\ell,0)^{\mathsf T}$, $(0,0,C\ell)^{\mathsf T}$, where A and C are fixed integers while the integer-valued dilution parameter ℓ will be taken to infinity. This case is obtained from that of a cubic lattice with the identifications

$$n_{\rm imp}\to\frac{1}{A^2\,C\,\ell^3},\qquad \alpha\to\frac{J_\parallel}{J_\perp}\frac{C^2}{A^2}, \tag{5.15}$$

in Eq. (5.12a) and (5.12b). Independently of the ratio C/A of the tetragonal superlattice, the Ising antiferromagnetic state AF(1) is favored over the Ising ferromagnetic state F.

The opposite conclusion is found, however, for dilute body-centered or face-centered tetragonal lattices. The difference arises because closest neighbors in these lattices have a stronger tendency to have ferromagnetic interactions than in simple tetragonal lattices. For the face-centered tetragonal lattice, the basis vectors are $(A,A,0)$, $(A,0,C)$, and $(0,A,C)$. The corresponding dual basis vectors in reciprocal space are $\boldsymbol{e}_1=\pi(1/A,1/A,-1/C)$, $\boldsymbol{e}_2=\pi(1/A,-1/A,1/C)$, and $\boldsymbol{e}_3=\pi(-1/A,1/A,1/C)$. Their linear combinations with integer coefficients span the reciprocal lattice $\mathcal{L}^\star$. It is convenient to represent a generic reciprocal lattice vector $\boldsymbol{G}\in\mathcal{L}^\star$ as $\boldsymbol{G}=n_1\,\boldsymbol{e}_1+n_2\,\boldsymbol{e}_2+n_3(\boldsymbol{e}_2+\boldsymbol{e}_3)$. With this choice, the asymptotic energy difference between the ferromagnetic and the antiferromagnetic states in the infinite dilution limit $n_{\rm imp}\to 0$ can be written as

$$\frac{\varepsilon_{\mathcal{L}}^{\rm F}-\varepsilon_{\mathcal{L}}^{\rm AF(1)}}{\gamma\, n_{\rm imp}}=\sum_{\boldsymbol{n}\in\mathbb{Z}^3}\frac{g_{\boldsymbol{n}+(\boldsymbol{e}_3/2)}-g_{\boldsymbol{n}}}{J_\perp}, \tag{5.16a}$$

where

$$g_{\boldsymbol{n}}\coloneqq\frac{(n_1-n_2-2n_3)^2}{\alpha\,[(n_1+n_2)^2+(n_1-n_2)^2]+(n_1-n_2-2n_3)^2}, \tag{5.16b}$$

with the convention $g_{\boldsymbol{0}}=1$. Carrying out the sum over n_3 one finds

$$\frac{\varepsilon_{\mathcal{L}}^{\rm F}-\varepsilon_{\mathcal{L}}^{\rm AF(1)}}{\gamma\, n_{\rm imp}}=\sum_{\boldsymbol{n}\in\mathbb{Z}^2\setminus\{\boldsymbol{0}\}}\frac{(-1)^{n_1-n_2}}{J_\perp}\times\frac{\pi\sqrt{2\alpha\,(n_1^2+n_2^2)}}{\sinh\left(\pi\sqrt{2\alpha\,(n_1^2+n_2^2)}\right)}. \tag{5.17}$$

For body-centered tetragonal lattices one finds the same expression, with the replacement $2\alpha\to\alpha$. The energy difference turns out to be always negative for any value of α, as seen in Fig. 10. Thus, in these lattices the ferromagnetic state is favored over the layered antiferromagnetic state.

B. Random, dilute impurities

Let us now turn to the case of randomly distributed impurities that occupy a fraction $n_{\rm imp}$ of the sites of the cubic host lattice Λ. We assume again that the relevant contenders for the ground state are given by configurations defined by Eqs. (5.1a) and (5.1b). In (5.1b), one should now set $\ell=1$, since only the lattice constant of the cubic host lattice Λ is relevant. These configurations are expected to come reasonably close to the true ground state and the relevant competing metastable configurations. However, it is clear that they will differ in the orientation of a few spins (the relative fraction of which is expected to becoming increasingly small as $n_{\rm imp}\to 0$) from the simple configurations (5.1a) and (5.1b). We will come back to this issue below.

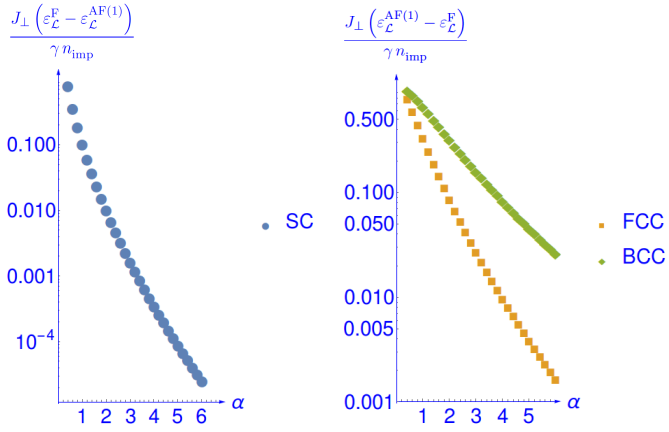

FIG. 10. (Color online) Dependence of the energy difference between the Ising ferromagnetic state (F) and antiferromagnetic state [AFM(1)] as a function of $\alpha \equiv J_\parallel/J_\perp$ for a simple cubic superlattice (right panel) in the large dilution limit. The left panel shows the energy difference between the Ising antiferromagnetic state [AF(1)] and ferromagnetic state (F) for face centered superlattices (yellow squares) and a body centered superlattice (green diamonds). Independently of the value of α, the antiferromagnetic state has lower energy for simple cubic superlattices while the ferromagnetic state has lower energy for face and body centered superlattices.

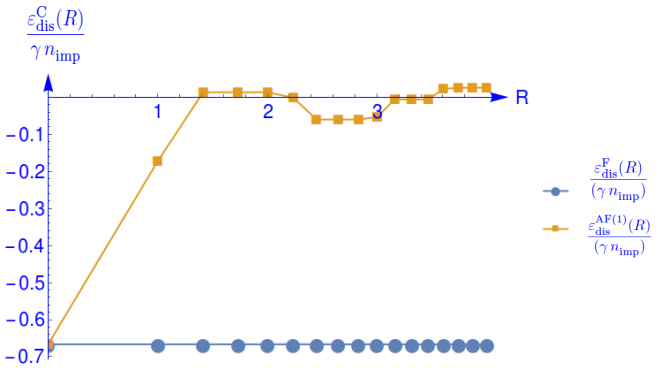

FIG. 11. (Color online) Dependence on R of $\varepsilon^{\rm C}_{\rm dis}(R)/(\gamma\, n_{\rm imp})$ defined in Eq. (5.19) for isotropic couplings $J_\perp = J_\parallel \equiv J$ for the ferromagnetic (C = F, blue dots) and the layered antiferromagnetic state (C = AF(1), yellow squares). Energies are given in units of J.

If the impurities are distributed randomly according to a Poisson process, the average energy per impurity bond of the trial states F and AF(m) is given by

$$\varepsilon^{\rm C}_{\rm dis} = -\gamma\, n_{\rm imp}\left(\sum_{\boldsymbol{r}\in\Lambda}\Gamma^{(0)}_{\boldsymbol{r}}\, f^{\rm C}(z) + \frac{1}{J_\perp}\delta_{\rm C,F}\right), \qquad (5.18)$$

since any site $\boldsymbol{r}$ of the cubic host lattice Λ is the lower end of an impurity bond with probability $n_{\rm imp}$, independently of the location of other impurities. From this observation, one might conclude that the antiferromagnetic state will dominate again. However, the above consideration does not treat correctly impurities located at short distances from each other. On the one hand, rare pairs of impurities that are located much closer to each other than the average separation $n_{\rm imp}^{-1/3}$ do not follow the pattern (5.1a) and (5.1b), but simply optimize their mutual interaction energy, irrespective of the global ordering pattern. Since such pairs nevertheless contribute a finite fraction to the total energy estimated above, they must be corrected for, which will turn out to favor the ferromagnetic ordering. This conclusion will become clear below, as a corollary to the discussion of another short-distance effect, which we will consider first.

Impurity distributions in real materials are usually not simply governed by a Poisson process, but rather, one should expect them to exhibit some short range correlations. For example, in the case of $YBaCuFeO_5$ impurity bonds arise due to chemical disorder which occasionally replaces the usual Cu-Fe pairs on bonds along its crystallographic c-axis by impurity configurations consisting in Fe-Fe or Cu-Cu pairs. Fe-Fe pairs differ from Fe-Cu pairs by the sign and magnitude of the resulting magnetic exchange constant. Moreover, both Fe-Fe and Cu-Cu pairs differ from Fe-Cu pairs in their local charge density. The resulting Coulomb repulsion between such impurity configurations thus suppresses the occurence of pairs of impurities at short distances. In a crude manner, we can mimic this effect by a hard constraint on the minimal distance between impurities, excluding distance vectors with $|\boldsymbol{r}| \le R$. With such a constraint the average energy per impurity (5.18) is modified to

$$\varepsilon^{\rm C}_{\rm dis}(R) = -\gamma\, n_{\rm imp}\left(\sum_{\substack{\boldsymbol{r}\in\Lambda\\ |\boldsymbol{r}|>R}}\Gamma^{(0)}_{\boldsymbol{r}}\, f^{\rm C}(z) + \frac{1}{J_\perp}\,\delta_{\rm C,F}\right). \qquad (5.19)$$

Note that for $R = 0$ these energies are simply $n_{\rm imp}$ multiplying the energy per impurity $\varepsilon^{\rm C}_{\mathcal{L}=\Lambda}(R)$ of a maximally dense system of impurities, cf. Eq. (5.2a). As we have shown in the previous section, those energies are all degenerate. Since the sum over $\boldsymbol{r}$ in Eq. (5.19) is dominated by small $|\boldsymbol{r}|$, even a small R of the order of one lattice constant will have a decisive effect and lift this degeneracy. In Fig. 11, we plot as a function of R the average energies $\varepsilon^{\rm F}_{\rm dis}(R)/(\gamma n_{\rm imp})$ and $\varepsilon^{{\rm AF}(m=1)}_{\rm dis}(R)/(\gamma n_{\rm imp})$ of the two most relevant competitor states. Already, for the smallest effective exclusion radius of $R \ge R_{\rm c} = 1$ (in units of the host cubic lattice spacing), we find that the ferromagnetic state (and thus XY spiral order) wins over the antiferromagnetic state (i.e., XY fan order). This numerical result can be understood by recalling that $\varepsilon^{\rm F}$ and $\varepsilon^{\rm AF(1)}$ are degenerate for $R = 0$. Upon barring impurities on nearest-neighbor sites on the host cubic lattice, the two states receive a relative energy shift $4n_{\rm imp}\Gamma_{\boldsymbol{r}=\boldsymbol{z}} = 4n_{\rm imp}\times(\frac{A}{J})$, which stabilizes the ferromagnetic state ($A \approx 0.123$). Larger exclusion radii

tend to reinforce this trend, as shown in Fig. 11. In the limit of large R, the energy per impurity bond of the ferromagnetic state is more favorable than that of the antiferromagnetic one by $\gamma n_{\rm imp} 2/(3J)$ in the case of isotropic couplings. This can be understood as follows: For isotropic couplings, the ferromagnetic energy per bond, $\varepsilon^{\rm F} = -\gamma n_{\rm imp} 2/(3J)$, remains invariant upon exclusion of interactions with a set of sites that is invariant under the cubic symmetry group, as can be seen in Fig. 11. In contrast, in an antiferromagnetic state, the interactions with the neighbors in thin spherical shells of approximately fixed radius $r > R$) come with alternating signs. Those tend to cancel the more effectively the larger is R, such that $\varepsilon^{\rm AF(1)}/n_{\rm imp}\gamma \to 0$ as $R \to \infty$.

Even without any repulsive short range correlations between impurity locations, one expects Ising ferromagnetism to prevail at sufficiently low impurity densities. This is because rare impurities with a neighboring impurity much closer than $n_{\rm imp}^{-1/3}$ should effectively be taken out of the calculation for the average energy. Indeed, if the close pair is antiferromagnetically coupled, it will form a singlet and essentially decouples from the global ordering pattern. If instead the pair is ferromagnetically coupled, it forms a bigger spin that can then be incorporated in the consideration like any other typical spin. The net effect of treating such close pairs in this way boils down to considering only original or effective spins with pairwise separations of the order of $R_{\rm eff} \gtrsim c\, n_{\rm imp}^{-1/3}$ with some constant c of order 1. The competition for the global ordering pattern then becomes essentially identical to the one of the constrained superlattice above, with $R_{\rm eff}$ now taking the role of the exclusion radius in Eq. (5.19). From these considerations we predict that for sufficiently dilute concentrations $n_{\rm imp} \lesssim (c/R)^3_{\rm c}$ the Ising ferromagnetic order prevails.

VI. CONCLUSION AND OUTLOOK

Any three-dimensional lattice hosting XY spins that interact through ferromagnetic nearest-neighbor exchange interactions display a ferromagnetic long-range order below some critical temperature. We have given sufficient conditions under which the replacement of a dilute fraction of the ferromagnetic by antiferromagnetic bonds destabilizes the ferromagnetic order in favor of non-colinear long-range order in the form of a spiral phase. A necessary but not sufficient condition for spiral order is that the antiferromagnetic exchanges along the impurity bonds be sufficiently larger than the ferromagnetic couplings, so as to induce canting, which eases the energetic cost due to the frustration. If this condition is met, a sufficient condition for spiral order is a strong correlation between the impurity bonds such that (i) they all point along a preferred direction and (ii) they are distributed in space such that ferromagnetic interactions dominate between the Ising degrees of freedom associated with the local canting patterns around the impurities. We showed rigorously that (ii) is satisfied for impurities located on Bravais superlattices with properties that favor spiral order: They are lattices whose shortest lattice vectors tend to point in directions in which the effective Ising interactions are ferromagnetic, while neighboring impurities along the z-axis, for which the interactions are antiferromagnetic, appear only at larger distance. Small deviations from such a Bravais lattice will not destroy the spiral order. However, we argued that completely randomly distributed impurities are prone to stabilize spiral order at low enough impurity density. At higher impurity density, a short ranged repulsion among impurity bonds, e.g. due to Coulomb constraints in real materials, has the main effect of reducing the stability of fan states (layered antiferromagnetic orderings of the canting degrees of freedom), and thus also stabilizes spiral order. Hence, once the orientational correlation (i) is ensured, the tendency towards spiral order is rather strong.

On the other hand, if the impurity bonds *and* their orientations are white-noise correlated in space, the microscopic XY Hamiltonian belongs to the family of three-dimensional XY gauge glasses introduced by Villain. Those host amorphous, glassy order. From this it follows that the zero-temperature phase diagram of two-dimensionalXY magnets (as characterized by the strength of the frustrating antiferromagnetic interactions and their spatial correlations) contains at least four stable phases: The ferromagnetic phase, the spiral phase, the fan phase (i.e., ferromagnetic in plane order with oscillating orientation from plane to plane), and the gauge glass phase.

All considerations so far apply at vanishing temperature. However, it is possible to make interesting predictions regarding the critical temperature $T_{\rm spi}$ below which the transition to the XY magnetic spiral occurs. For example, in the large dilution limit $n_{\rm imp} \ll 1$ of the impurity bonds we can make the following prediction relying on dimensional analysis. In the dilute limit, the characteristic dimensionless interaction strength between Ising spins is proportional to $n_{\rm imp}$. This implies that the temperature $T_{\rm spi}$ at which the transition to the XY magnetic spiral occurs is also proportional to the fraction $n_{\rm imp}$ of impurity bonds. As the spiral wave vector $Q^{\rm min}$ in the ground state was shown to be proportional to $n_{\rm imp}$, the ratio $T_{\rm spi}/Q^{\rm min}$ is predicted to be a $n_{\rm imp}$-independent constant by this argument. Measuring this constant provides an independent estimate of the characteristic strength of the magnetic couplings driving the transition to the magnetic spiral order.

This qualitative argument can be refined by a mean-field estimate of $T_{\rm spi}$. We start from the effective Ising model (3.40) that is valid for a dilute fraction $n_{\rm imp}$ of impurity bonds at temperatures well below the ferromagnetic ordering temperature in the clean limit $n_{\rm imp} = 0$. We replace this Ising Hamiltonian by the mean-field Hamiltonian

$$H_{\mathcal{L}}^{\rm MF} \coloneqq -\sum_{\tilde{\boldsymbol{r}} \in \mathcal{L}} B_{\tilde{\boldsymbol{r}}}^{\rm MF}\, \sigma_{\tilde{\boldsymbol{r}}}, \tag{6.1a}$$

where the effects on $\sigma_{\tilde{\boldsymbol{r}}}$ from all the Ising spins $\sigma_{\tilde{\boldsymbol{r}}'}$ is approximately captured by the mean-field magnetic field

$$B^{\rm MF}_{\tilde{\boldsymbol{r}}} \coloneqq \sum_{\tilde{\boldsymbol{r}}'\in\mathcal{L}\setminus\{\tilde{\boldsymbol{r}}\}} J^{(\rm I)}_{\tilde{\boldsymbol{r}}-\tilde{\boldsymbol{r}}'} \langle\sigma_{\tilde{\boldsymbol{r}}'}\rangle_{\rm MF} \tag{6.1b}$$

subject to the non-linear constraint

$$\langle\sigma_{\tilde{\boldsymbol{r}}}\rangle_{\rm MF} = \tanh\left(\beta \sum_{\tilde{\boldsymbol{r}}'\in\mathcal{L}\setminus\{\tilde{\boldsymbol{r}}\}} J^{(\rm I)}_{\tilde{\boldsymbol{r}}-\tilde{\boldsymbol{r}}'} \langle\sigma_{\tilde{\boldsymbol{r}}'}\rangle_{\rm MF}\right), \tag{6.1c}$$

where β is the inverse temperature in units where the Boltzmann constant set to unity. Such a mean-field approximation is justified by the long-range nature of the dipolar interaction and the dimensionality of space (i.e., three, which is here the upper critical dimension[23–27]). We assume isotropic boundary conditions and interactions and the Ising ferromagnetic state (5.1a) for $\langle\sigma_{\tilde{\boldsymbol{r}}}\rangle_{\rm MF}$. We use the lattice sum rules (5.3) and (5.4) to estimate the mean-field magnetic field (6.1b). The onset of Ising ferromagnetism (spiral order in the original XY spin degrees of freedom) is then obtained by solving for $1/\beta$ the linearized version of Eq. (6.1c), i.e.,

$$T^{\rm MF}_{\rm spi} = \frac{\big(|J_{\rm imp}|+J\big)^2\,\sin^2\Delta\theta}{3J}\,n_{\rm imp}, \tag{6.2}$$

where $\Delta\theta$ is the positive solution to Eq. (3.6d) at the isotropic point $J_\perp = J_\parallel \equiv J$. On the other hand, Eq. (4.6c) predicts for the ferromagnetic state that

$$|Q^{\rm min}| = \frac{\big(|J_{\rm imp}|+J_\perp\big)\,\sin\Delta\theta}{J_\perp}\,n_{\rm imp} \tag{6.3}$$

for any anisotropy. When $J_\perp = J_\parallel \equiv J$ holds, the ratio

$$\frac{T^{\rm MF}_{\rm spi}}{|Q^{\rm min}|} = \frac{\big(|J_{\rm imp}|+J\big)\,\sin\Delta\theta}{3} \tag{6.4}$$

follows.

For small concentrations $n_{\rm imp} \ll 1$, Eq. (6.2) is to be interpreted as follows from the perspective of the original microscopic XY spin degrees of freedom entering Hamiltonian (2.1). Upon lowering the temperature in the XY paramagnetic phase, a continuous phase transition takes place in the three-dimensional XY universality class to a ferromagnetic phase at the temperature T_{XY}. This ferromagnetic phase is unstable at the temperature $T_{\rm spi} \ll T_{XY}$ through a continuous phase transition to a XY spiral phase driven by the dilute concentration $n_{\rm imp} \ll 1$ of impurity bonds that are orientationally correlated and for which $T_{\rm spi}$ is of the order of the mean-field transition temperature (6.2). The spiral wavevector $Q^{\rm min}$ may serve as an order parameter for this Ising transition. The associated critical exponents are expected to assume mean field values, given the dimensionality and the long range nature of the dipolar interactions.

What can we say if $n_{\rm imp}$ is increased so that $T^{\rm MF}_{\rm spi} \sim T_{XY}$? In this limit, the effective Ising model (3.40) is not anymore a valid approximation of Hamiltonian (2.1). However, it might happen that there is a direct transition from the paramagnetic phase to an ordered phase with an incommensurate magnetic spiral that is driven by a large concentration $n_{\rm imp} \lesssim 1$ of impurity bonds that are orientationally correlated. An approach that is nonperturbative in $n_{\rm imp}$ is needed to address the existence of such a direct phase transition driven by strong disorder.

In the companion paper Ref. 17, it is argued that $YBaCuFeO_5$ unites all the essential ingredients of the Hamiltonian discussed in this work, and thus could realize the spiral XY phase described above. The supporting evidence is as follows. On the one hand, Monte Carlo simulations for realistic values of the magnetic exchange couplings in $YBaCuFeO_5$ yield transition temperatures to the magnetic spiral phase as high as 250 K. On the other hand, it was reported in Ref. 28 that tuning the degree of occupational disorder by changing the annealing procedure of $YBaCuFeO_5$ affects the transition temperature and the wave vector of the spiral in a way that is qualitatively consistent with Eq. (6.4).

The main physical mechanism we discussed in this work also applies to other systems. First, we point out that the restriction to XY spins is not essential. Indeed, we expect that Heisenberg spins with an $O(3)$ symmetry (or any other set of continuous degrees of freedom undergoing spontaneous symmetry breaking) would exhibit essentially the same phenomenology: At low temperatures the unfrustrated system will order ferromagnetically. Frustrating antiferromagnetic impurity bonds induce local canting patterns that are subject to effective pairwise interactions. The canting pattern around an impurity spontaneously breaks not only the inversion symmetry with respect to the center of the impurity bond, but also the rotational symmetry around its axis; as a consequence, in contrast to the case of XY spins, where the cantings have a single discrete Ising degree of freedom, the canting patterns in Heisenberg magnets will be associated with a continuous (XY-like) degree of freedom. Upon integrating out spin waves, we expect an effective XY model of cantings to emerge, a ferromagnetic order which again implies spiral order for the original Heisenberg spins.

The phenomenology of XY spins immediately carries over to superconducting systems, too. There, the role of XY spins is taken by superconducting islands with a well established amplitude of the superconducting order parameter. Josephson couplings then replace the magnetic exchange couplings. Frustration could be induced by Josephson couplings with the opposite sign (based on ferromagnetic materials for example). However, a much simpler way to achieve frustration consists in threading a homogenous magnetic flux through a Josephson junction array. The recent advances in fabrication techniques and nanolithography for such devices will allow to the artifically design and control XY systems with any de-

sired spatial pattern of frustrated plaquettes that truthfully emulate the presence of antiferromagnetic impurity bonds in the magnetic analogue. A magnetic spiral phase with ferromagnetic order of the Ising degrees of freedom of the canting patterns then translates into a system of vortices with uniform charge (sense of circulation), entailing a global supercurrent in the system. This will be explored in future work.

ACKNOWLEDGMENTS

This research was partially supported by NCCR MARVEL, funded by the Swiss National Science Foundation. We would like to thank N. Spaldin, M. Troyer, M. Medarde, M. Kenzelman, and M. Morin for useful discussions. H.S. acknowledges support from the DFG via FOR 1346, the SNF Grant 200021E-149122, ERC Advanced Grant SIMCOFE, ERC Consolidator Grant CORRELMAT (project number 617196). This work was supported by JSPS KAKENHI Grant Numbers 16H01064 (J-Physics), 16K17735.

Appendix A: Lattice sum

Let us consider a maximally dense lattice of impurity bonds, i.e., $\mathcal{L} = \Lambda$ with Λ the host cubic lattice. By comparing the interaction energies of various candidates for ground states we will establish that, in the dense limit, an infinite family of states are degenerate, namely all those in which the Ising degrees of freedom within any xy- plane of the cubic lattice are ferromagnetically ordered, however, with a completely arbitrary polarization pattern in the direction perpendicular to the planes,

$$\sigma_{\boldsymbol{r}} \equiv s_z = \pm 1. \tag{A1}$$

According to Eq. (3.40), up to a global constant, the total energy per lattice site of such a configuration is

$$\begin{aligned}\varepsilon[s_z] &\equiv \frac{E[s_z]}{N} \\ &= -\frac{1}{2}\left(|J_{\mathrm{imp}}| + J_\perp\right)^2 \sin^2\Delta\theta \\ &\quad \times \frac{1}{|\Lambda|}\sum_{\boldsymbol{r}',\boldsymbol{r}''\in\Lambda} J_{\boldsymbol{r}'-\boldsymbol{r}''}\, s_{z'}\, s_{z''}\end{aligned} \tag{A2a}$$

with

$$\begin{aligned}J_{\boldsymbol{r}'-\boldsymbol{r}''} &= \frac{J^{(\mathrm{I})}_{\boldsymbol{r}'-\boldsymbol{r}''}}{\left(|J_{\mathrm{imp}}| + J_\perp\right)^2 \sin^2\Delta\theta} \\ &= \Gamma^{(0)}_{\boldsymbol{r}'-\boldsymbol{r}''} + \frac{1}{J_\perp\,|\Lambda|}.\end{aligned} \tag{A2b}$$

Assumption (A1) allows to make the following useful manipulations. We start from

$$\sum_{\boldsymbol{r}',\boldsymbol{r}''\in\Lambda} J_{\boldsymbol{r}'-\boldsymbol{r}''}\, s_{z'}\, s_{z''} \equiv \sum_{x',y',z'}\sum_{x'',y'',z''} J_{\boldsymbol{r}'-\boldsymbol{r}''}\, s_{z'}\, s_{z''}. \tag{A3}$$

We then do the planar sums over x', y' and x'', y'' holding z' and z'' fixed. The right-hand side becomes

$$\sum_{z'}\sum_{z''}\left(\sum_{x',y'}\sum_{x'',y''} J_{(x'-x'',y'-y'',z'-z'')^{\mathsf{T}}}\right) s_{z'}\, s_{z''}. \tag{A4}$$

The double sum over the planar coordinates can be decomposed into a sum over center of mass and relative coordinates. Because the kernel only depends on the relative coordinates, we may write for the right-hand side

$$\sum_{z'}\sum_{z''}\left(L_x\, L_y \sum_{x,y} J_{(x,y,z)^{\mathsf{T}}}\delta_{z,z''-z'}\right) s_{z'}\, s_{z''}. \tag{A5}$$

Here, we have assumed that the cubic lattice Λ is comprised of $|\Lambda| = L_x \times L_y \times L_z$ sites $\boldsymbol{r} = (x,y,z)^{\mathsf{T}}$.

We now consider the field $B_{z''|z'}$ exerted by a fully positively magnetized plane with z-coordinate z' ($s_{z'} = 1$) on any spin in a plane with z-coordinate z''. Up to the multiplicative constan $L_x\, L_y$, this field is nothing but the parenthesis in Eq. (A5). We now show that $B_{z''|z'}$ vanishes except if the planes are the same, i.e., $z' = z''$. In other words, the planes are mutually decoupled. To establish this claim, we compute

$$\begin{aligned}B_{z''|z'} &\coloneqq \sum_{\boldsymbol{r}\in\Lambda} \delta_{z,z''-z'}\, J_{\boldsymbol{r}} \\ &= \sum_{\boldsymbol{r}\in\Lambda} \delta_{z,z''-z'}\, \frac{1}{|\Lambda|}\sum_{\boldsymbol{k}\in \mathrm{BZ}(\Lambda)\setminus\{\boldsymbol{0}\}} \Gamma^{(0)}_{\boldsymbol{k}} e^{\mathrm{i}\boldsymbol{k}\cdot\boldsymbol{r}} + \frac{1}{J_\perp\, L_z}.\end{aligned} \tag{A6}$$

The sums over the x- and y-coordinates deliver

$$B_{z''|z'} = \sum_z \frac{\delta_{z,z''-z'}}{J_\perp\, L_z} \sum_{\substack{k_z \\ k_z \boldsymbol{e}_z\in \mathrm{BZ}(\Lambda)\setminus\{\boldsymbol{0}\}}} e^{\mathrm{i}k_z\, z} + \frac{1}{J_\perp\, L_z}. \tag{A7}$$

Here, $\boldsymbol{e}_x$, $\boldsymbol{e}_y$, and $\boldsymbol{e}_z$ define a basis of the Brillouin zone BZ for $|\Lambda| < \infty$ and we use the fact that $\Gamma^{(0)}_{\boldsymbol{k}} = 1/J_\perp$ when $k_x = k_y = 0$, $k_z \neq 0$ according to Eq. (5.6). The sum over z is easily performed,

$$B_{z''|z'} = \frac{1}{J_\perp\, L_z}\left(\sum_{\substack{k_z \\ k_z \boldsymbol{e}_z\in \mathrm{BZ}(\Lambda)\setminus\{\boldsymbol{0}\}}} e^{\mathrm{i}k_z\,(z'-z'')} + 1\right). \tag{A8}$$

The sum over k_z delivers our claim

$$B_{z''|z'} = \frac{\delta_{z',z''}}{J_\perp}. \tag{A9}$$

If we combine Eqs. (A2), (A5), (A6), and (A9), we find that the energy per spin in all layered state of ferromagnetically ordered planes is the constant independently of the magnetization structure s_z.

$$\varepsilon[s_z] = -\frac{1}{2}\frac{\left(|J_{\rm imp}| + J_\perp\right)^2 \sin^2\Delta\theta}{J_\perp}, \qquad \text{(A10)}$$

* andrea.scaramucci@psi.ch
† shinaoka@itp.phys.ethz.ch

[1] H. Katsura, N. Nagaosa, and A. V. Balatsky, Phys.Rev. Lett. **95**, 057205 (2005).
[2] S.-W. Cheong and M. Mostovoy, Nat Mater **6**, 13 (2007).
[3] D. Khomskii, Physics **2** (2009).
[4] Y. Tokura and S. Seki, Adv, Mat. **22**, 1554 (2010).
[5] M. Kenzelmann, A. B. Harris, S. Jonas, C. Broholm, J. Schefer, S. B. Kim, C. L. Zhang, S.-W. Cheong, O. P. Vajk, and J. W. Lynn, Phys. Rev. Lett. **95**, 087206 (2005).
[6] T. Goto, T. Kimura, G. Lawes, A. P. Ramirez, and Y. Tokura, Phys. Rev. Lett. **92**, 257201 (2004).
[7] M. Mochizuki and N. Furukawa, Phys. Rev. B **80**, 134416 (2009).
[8] D. H. Lyons and T. A. Kaplan, Phys. Rev. **120**, 1580 (1960).
[9] N. B. Ivanov, S. E. Krger, and J. Richter, Phys. Rev. B **53**, 2633 (1996).
[10] D. E. Cox, W. J. Takei, and G. Shirane, J. Phys. Chem. Solids **24**, 405 (1963).
[11] S. Utsumi, D. Yoshiba, and N. Momozawa, J. Phys. Soc. Jpn. **76**, 034704 (2007).
[12] M. Morin, A. Scaramucci, M. Bartkowiak, E. Pomjakushina, G. Deng, D. Sheptyakov, L. Keller, J. Rodriguez-Carvajal, N. A. Spaldin, M. Kenzelmann, K. Conder, and M. Medarde, Phys. Rev. B **91**, 064408 (2015).
[13] B. Kundys, A. Maignan, and C. Simon, Appl. Phys. Lett. **94**, 072506 (2009).
[14] V. Caignaert, I. Mirebeau, F. Boure, N. Nguyen, A. Ducouret, J.-M. Greneche, and B. Raveau, J. Solid State Chem. **114**, 24 (1995).
[15] Y. Kawamura, T. Kai, E. Satomi, Y. Yasui, Y. Kobayashi, M. Sato, and K. Kakurai, J. Phys. Soc. Jpn. **79**, 073705 (2010).
[16] M. J. Ruiz-Aragón, E. Morán, U. Amador, J. L. Martnez, N. H. Andersen, and H. Ehrenberg, Phys. Rev. B **58**, 6291 (1998).
[17] A. Scaramucci, H. Shinaoka, M. V. Mostovoy, M. Müller, C. Mudry, M. Troyer, and N. A. Spaldin, "Multiferroic magnetic spirals induced by random magnetic exchanges," (2016), arXiv:1610.00783.
[18] J. J. Alonso and J. F. Fernández, Phys. Rev. B **81**, 064408 (2010).
[19] J. F. Fernández and J. J. Alonso, Phys. Rev. B **79**, 214424 (2009).
[20] J. Villain, Journal de Physique **36**, 581 (1975).
[21] J. Villain, J. Phys. C: Solid State Physics **10**, 4793 (1977).
[22] J. Villain, J. Phys. C: Solid State Physics **11**, 745 (1978).
[23] A. I. Larkin and D. E. Khmel'nistskiĭ, Sov. Phys. jetp **29**, 1123 (1969).
[24] M. H. Cohen and F. Keffer, Phys. Rev. **99**, 1128 (1955).
[25] A. Aharony and M. E. Fisher, Phys. Rev. B **8**, 3323 (1973).
[26] A. Aharony, Phys. Rev. B **8**, 3342 (1973).
[27] A. Aharony, Phys. Rev. B **8**, 3349 (1973).
[28] M. Morin, E. Canvet, A. Raynaud, M. Bartkowiak, D. Sheptyakov, V. Ban, M. Kenzelmann, E. Pomjakushina, K. Conder, and M. Medarde, "Tuning magnetic spirals beyond room temperature with chemical disorder," (2016), arXiv:1608.03372.